Metastatic Tumor Growth in Steatotic Liver is Promoted by HAS2-Mediated Fibrotic Tumor Microenvironment

Yoon Mee Yang[1,2,3,4#], Jieun Kim[1,#], Zhijun Wang[1,5,##], Jina Kim[6,7,8,##], So Yeon Kim[1], Gyu Jeong Cho[2,4], Jee Hyung Lee[2], Sun Myoung Kim[2,4], Takashi Tsuchiya[1], Michitaka Matsuda[1], Vijay Pandyarajan[1], Stephen J. Pandol[1], Michael S. Lewis[9,10], Alexandra Gangi[11], Paul W. Noble[12], Dianhua Jiang[12], Akil Merchant[6,13], Edwin M. Posada[6,14], Neil A. Bhowmick[6,14], Shelly C. Lu[1], Sungyong You[6,7,8,*], Alexander M. Xu[6,15,16,*], Ekihiro Seki[1,6,15,*]

[1]Karsh Division of Gastroenterology and Hepatology, Department of Medicine, Cedars-Sinai Medical Center, Los Angeles, CA 90048, USA, [2]Department of Pharmacy, Kangwon National University, Chuncheon 24341, South Korea, [3]Multidimensional Genomics Research Center, Kangwon National University, Chuncheon 24341, Republic of Korea, [4]Innovative Drug Development Research Team for Intractable Diseases (BK21 plus), Kangwon National University, Chuncheon, 24341, Republic of Korea, [5]Division of Gastroenterology, Union Hospital, Tongji Medical College, Huazhong University of Science and Technology, Wuhan, China, [6]Samuel Oschin Comprehensive Cancer Institute, Cedars-Sinai Medical Center, Los Angeles, CA 90048, USA, [7]Department of Urology, Cedars-Sinai Medical Center, Los Angeles, CA 90048, USA, [8]Department of Computational Biomedicine, Cedars-Sinai Medical Center, Los Angeles, CA 90048, USA, [9]Department of Pathology, Cedars-Sinai Medical Center, Los Angeles, CA 90048, USA, [10]Department of Pathology, Veterans Affairs Greater Los Angeles Health Care System, Los Angeles, CA 90073, USA, [11]Department of Surgery, Cedars-Sinai Medical Center, Los Angeles, CA 90048, USA, [12]Department of Medicine and Women's Guild Lung Institute, Cedars-Sinai Medical Center, Los Angeles, CA 90048,USA, [13]Division of Hematology and Cellular Therapy, Department of Medicine, Cedars-Sinai Medical Center, Los Angeles, CA 90048, USA, [14]Division of Medical Oncology, Department of Medicine, Cedars-Sinai Medical Center, Los Angeles, CA 90048, USA, [15]Department of Biomedical Sciences, Cedars-Sinai Medical Center, Los Angeles, CA 90048, USA, [16]Fischell Department of Bioengineering, A. James Clark School of Engineering, University of Maryland, College Park, MD 20742

# YMY and Jieun K are the co-first authors and contributed equally to this work.
ZW and Jina K contributed equally as the second authors of this work.

***Correspondence to:**
Ekihiro Seki, M.D., Ph.D.
Karsh Division of Gastroenterology and Hepatology, Department of Medicine,
Cedars-Sinai Medical Center
8700 Beverly Blvd., Davis Research Bldg., Suite 2099, Los Angeles, CA 90048
Phone: +1-310-423-6605
Fax: +1-310-423-0157
E-mail: Ekihiro.Seki@cshs.org

Alexander M. Xu, PhD
Fischell Department of Bioengineering, A. James Clark School of Engineering,
University of Maryland
8728 Paint Branch Drive, College Park, MD 20742
E-mail: alexmxu@umd.edu

Sungyong You, PhD
Department of Urology and Computational Medicine
Cedars-Sinai Medical Center
8700 Beverly Blvd., Davis Research Bldg., Suite 2099, Los Angeles, CA 90048
E-mail: Sungyong.You@cshs.org

The authors have declared that no conflict of interest exists.

Abstract

Steatotic liver enhances liver metastasis of colorectal cancer (CRC), but this process is not fully understood. Steatotic liver induced by a high-fat diet increases cancer-associated fibroblast (CAF) infiltration and collagen and hyaluronic acid (HA) production. We investigated the role of HA synthase 2 (HAS2) in the fibrotic tumor microenvironment in steatotic liver using *Has2*$^{\Delta HSC}$ mice, in which *Has2* is deleted from hepatic stellate cells. *Has2*$^{\Delta HSC}$ mice had reduced steatotic liver-associated metastatic tumor growth of MC38 CRC cells, collagen and HA deposition, and CAF and M2 macrophage infiltration. We found low-molecular-weight HA activates yes-associated protein (YAP) in cancer cells, which then releases connective tissue growth factor to further activate CAFs for HAS2 expression. Single-cell analyses revealed a link between CAF-derived HAS2 with M2 macrophages and CRC cells through CD44; these cells associated with exhausted CD8 T cells via programmed death-ligand 1 and programmed cell death protein 1 (PD-1). HA synthesis inhibitors reduced steatotic liver-associated metastasis of CRC, YAP expression, CAF, M2 macrophage infiltration, and improved response to anti-PD-1 antibody. In conclusion, steatotic liver modulates a fibrotic tumor microenvironment to enhance metastatic cancer activity through a bidirectional regulation between CAFs and metastatic tumors, enhancing the metastatic potential of CRC in the liver.

Keywords: colorectal cancer, cancer-associated fibroblast, connective tissue growth factor, extracellular matrix, YAP

Introduction

Colorectal cancer (CRC) metastasizes most commonly to the liver, mainly through the portal vein(1). Once liver metastasis occurs, the five-year survival rate of patients with CRC drops from approximately 60% to 13%(2,3). Thus, liver metastasis is a major prognostic factor in patients with CRC(1,4). Although surgical resection is the primary treatment for CRC, only limited cases are considered for CRC resection after liver metastasis occurs(3,5). In most cases, chemotherapy is the standard care option for patients with CRC and liver metastasis(1,5).

Obesity is a serious health concern worldwide and is associated with the increased prevalence of metabolic dysfunction-associated steatotic liver disease (MASLD). MASLD is a common risk factor for primary liver cancer and other primary cancers, such as CRC, pancreatic cancer, prostate cancer, and breast cancer in humans and rodents(6-8). Clinical studies determined the association of obesity and MASLD with enhancement of CRC liver metastasis(9-12). Furthermore, our previous studies demonstrated the role of steatotic liver-derived extracellular vesicles and an immunosuppressive tumor microenvironment (TME) in the progression of CRC liver metastasis(13,14). However, the underlying mechanism by which the remodeling of the fibrotic immune microenvironment by steatotic liver contributes to CRC liver metastasis is not fully understood.

Hepatic stellate cells (HSCs) are the primary source of cancer-associated fibroblasts (CAFs) that are a component of the TME in the metastatic locus in the liver(15-19). CAFs transdifferentiate into a myofibroblastic form to produce extracellular matrix (ECM), such as collagen and hyaluronic acid (HA), that modulate the prometastatic TME. The effect of ECM on cancer growth is still not fully understood. We previously determined that in liver fibrosis, HA is

produced from activated HSCs through the upregulation of a HA synthase HAS2(20). We determined that low molecular weight (LMW) HA is a dominant form in the fibrotic liver, and proinflammatory and profibrogenic, which activates CD44, Toll-like receptor 4 (TLR4), and Notch signaling. In contrast, high MW (HMW) HA is anti-inflammatory and antifibrotic(20). Likewise, the size-dependent effect of HA is observed in cancers. In breast cancer, LMW-HA activates tumor-promoting signaling through CD44 and Yes-associated protein (YAP), but HMW-HA does not (21). In the present study, we hypothesize that HSC-derived CAFs upregulate HAS2 to produce HA, which promotes CRC liver metastasis. We determined that fibrotic TME associated with HAS2 and HA is increased and plays an important role in the steatotic liver compared with the non-steatotic liver using a mouse model and patient specimens. We found that a fibrotic TME and HAS2 contribute to YAP activation in cancer cells and the development of a prometastatic immunosuppressive TME comprising M2 tumor-associated macrophages (TAMs) and exhausted CD8 T cells. Lastly, we found the drugs that inhibit HA synthesis reduced metastatic tumor burden in steatotic liver in mice, and enhanced anti-tumor response when added anti-PD-1 therapy. Our study provides evidence of different tumor-promoting mechanisms in patients with liver metastasis in the presence and absence of steatotic liver; we propose that disease management of patients with CRC liver metastasis should differ, depending on whether or not they have steatotic liver disease.

Results

Increased fibrotic TME with upregulation of HAS2 and HA in CRC liver metastasis enhanced by HFD

To assess the impact of steatotic liver on metastatic CRC growth in the liver, C57BL/6 male wild-type (WT) mice were fed a low-fat diet (LFD) or a high-fat diet (HFD) for 8 weeks. After the sixth week of diet feeding, MC38 cells, a murine CRC cell line, were intrasplenically injected into the mice to form liver metastases (Figure 1A)(13,14). The area of the liver tumors was significantly larger in mice fed an HFD compared with those fed an LFD (Figure 1, B and C). RNA-seq and gene set enrichment analysis revealed that the gene signatures of extracellular matrix (ECM) organization, binding, assembly, collagen-containing ECM, and hepatic fibrosis were enriched in metastatic tumors from HFD-fed mice (Figure 1D). These data indicate that steatotic liver favors creation of a fibrotic TME. Therefore, we assessed the fibrotic TME by examining myofibroblastic CAF infiltration and deposition of ECM collagen and HA. A heat map showed genes associated with HA synthesis and metabolism were differentially expressed in tumors of mice fed an HFD compared with those fed an LFD (Figure 1E). Myofibroblastic CAF infiltration (as demonstrated by alpha-smooth muscle actin [α-SMA] expression) and collagen and HA deposition were increased in tumors of mice fed an HFD compared with those fed an LFD (Figure 1F). Next, we investigated the involvement of HA deposition in tumors. Among the three hyaluronan synthase (HAS) isoforms, *Has2* mRNA expression showed the greatest increase in the tumors from HFD-fed mice compared with LFD-fed mice (Figure 1G and Supplemental Figure 1A). RNAscope analysis showed increased *Has2* mRNA expression in HSCs of tumors from HFD-fed mice compared with LFD-fed mice (Figure 1H, Supplementary Figure 1, B and

C). We also validated the effect of steatosis on liver metastasis from other CRC and pancreatic cancers. These models also show increased tumor growth, ECM, HA deposition, and *Has2* expression by HFD feeding (Supplemental Figure 1, D and E).

We then validated the source of intra-tumoral CAFs using mice that expressed tdTomato under control of lecithin-retinol acyltransferase (Lrat)-Cre, which traces the HSC lineage(17-19,22). Lrat-tdTomato-positive CAFs were increased in the tumor after HFD feeding, indicating HSCs are the major source of intra-tumoral CAFs (Supplemental Figure 1, F). The expression of CD44, a receptor for HA, was increased in tumors from mice fed an HFD (Supplemental Figure 1G). These findings suggest that fibrotic TME and HSC-derived CAFs in liver metastases promote tumor growth in steatotic liver, and that HSC-derived HAS2 and HA-mediated CD44 activation could play a role in developing a metastatic TME in steatotic liver.

Loss of HSC-specific *Has2* reduces steatotic liver-enhanced metastatic liver tumor growth

To determine how a fibrotic TME plays a role in steatotic liver-associated liver metastasis, we studied an ECM component, HA, a signaling molecule that activates cancer-promoting pathways, including CD44. Because HAS2 is the most upregulated HAS enzyme in steatotic liver-associated liver metastasis (Figure 1G, and Supplemental Figure 1A) and HSCs are the cells responsible for expressing HAS2 and are the source of CAFs in the liver(20), we examined the contribution of HSC-derived HAS2 in metastatic liver tumor growth in the presence of steatotic liver using HSC-specific *Has2*-knockout ($Has2^{\Delta HSC}$) mice. Liver metastasis was evaluated 2 weeks after MC38 CRC cell inoculation in mice fed an LFD or an HFD. The liver

tumor formation was similar in WT and *Has2*$^{\Delta HSC}$ mice fed an LFD; tumor growth was increased in WT mice fed an HFD compared with WT mice fed an LFD; and in mice fed an HFD, tumor growth was significantly decreased in *Has2*$^{\Delta HSC}$ mice compared with WT mice (Figure 2, A-C, and Supplemental Figure 2A). The HA deposition was similar between WT and *Has2*$^{\Delta HSC}$ mice fed an LFD, but the HA deposition increased in HFD-fed mice, which was reduced by HSC-specific *Has2* deletion (Figure 2, D and E). Similarly, α-SMA expression and collagen content, representing myofibroblastic CAFs, were decreased in HFD-fed *Has2*$^{\Delta HSC}$ mice compared with HFD-fed WT mice (Figure 2, D and E), suggesting HAS2 is crucial for developing myofibroblastic CAFs and collagen production in tumor lesions when coexistent with steatotic liver. Fat deposition developed similarly in the livers from WT and *Has2*$^{\Delta HSC}$ mice fed an HFD (Supplemental Figure 2B). These results suggest that HAS2-mediated fibrotic TME plays an important role in metastatic tumor growth in the presence of steatosis. We then examined whether HA deposition contributes to the early engraftment of tumor cells to the liver by assessing liver tumors on day 3 after tumor inoculation. While we did not observe HA deposition on day 3, tumor numbers were higher in steatotic livers (Supplemental Figure 2, C and D). In addition, inhibition of HA synthesis by 4-methylumbelliferone (4-MU) did not affect the engraftment (Supplemental Figure 2, E-F). These results indicate that tumor engraftment occurred prior to HA deposition.

LMW-HA regulates the Hippo-YAP pathway in CRC liver metastasis

Although our previous study demonstrated steatotic liver-derived extracellular vesicles regulate

YAP signaling through their cargo microRNAs(14), we sought to determine whether HA also plays a role in YAP activation. HA can be formed in different sizes HMW-HA and LMW-HA, generated by hyaluronidases(23). After binding to HA receptors, such as CD44, HMW-HA and LMW-HA differentially regulate YAP signaling(21). HA concentrations in the serum and tumor are significantly higher in tumor-bearing mice fed an HFD than an LFD (Figure 3A). Under the HFD condition, LMW-HA is higher than other forms of HA in the serum and tumor of mice bearing metastatic liver tumors (Figure 3B). We determined that the expression of HA receptors CD44 and TLR4 was significantly increased in tumors from mice fed an HFD compared with an LFD, suggesting that HA receptor signaling is augmented in liver metastasis under steatotic liver conditions (Supplemental Figures, 1G and 3A). LMW-HA treatment induced proliferation and invasive capacity along with mRNA upregulation of *Yap1* and its target *Ccn2* in MC38 CRC cells, whereas HMW-HA treatment had no effect (Figure 3, C-E). *Ccn2* expression was positively correlated with LMW-HA in mouse metastatic liver tumors (Figure 3F). Correlation of YAP target genes, such as *Ccn2*, *Ccn1*, *Axl*, and *Ankrd1*, with *Has2* mRNA expression was also observed (Supplemental Figure 3B). Furthermore, nuclear translocation of YAP and mRNA expression of *Yap1* and *Ccn2* were decreased in tumors from $Has2^{\Delta HSC}$ mice fed an HFD, suggesting a role of HAS2 and HA in the activation of YAP (Figure 3G and Supplementary Figure 3C). Subsequently, we investigated the mechanism of LMW-HA-induced YAP activation. FAK phosphorylates YAP at tyrosine 357 residues, resulting in YAP nuclear translocation(24). We examined whether FAK is involved in LMW-HA-induced YAP activation using a FAK inhibitor. FAK inhibition suppressed LMW-HA-induced nuclear translocation of YAP (Supplemental Figure 3, D and E). Lastly, we validated the role of YAP in HA-mediated cancer activity. *Yap1* silencing using short hairpin RNA in MC38 CRC cells reduced LMW-HA-induced

CRC invasion (Figure 3H), indicating that YAP plays a role in HA-mediated CRC invasion. All these findings support the mechanism by which HAS2 and LMW-HA regulate YAP signaling to promote metastatic CRC activities under steatotic liver conditions.

Cancer YAP signaling mediates HAS2 expression and myofibroblastic CAF development

YAP is considered to be a master regulator in cancer, providing many malignant attributes(25). Our data demonstrate that YAP is a key downstream effector of HA signaling, promoting cancer activity (Figure 3). To further analyze the role of YAP in CRC liver metastasis enhanced by steatosis, *Yap1* was silenced in MC38 CRC cells and was used for the steatotic liver-associated liver metastasis model. Consistent with our previous study (14), we observed similar results that *Yap1* silencing in MC38 CRC cells reduced metastatic tumor growth enhanced by HFD feeding (Figure 4A). These newly obtained data validate our prior findings in an independent set of experiments. Bulk RNA-seq analysis revealed the ECM-related gene signatures were reduced when *Yap1* was silenced (Figure 4B), indicating that the cancer-derived YAP signaling not only acts as a downstream effector of HA but also promotes CAF activity to regulate a fibrotic TME. Collagen deposition and myofibroblastic CAF infiltration were reduced by knocking down *Yap1* in tumors of steatotic liver as assessed by Sirius red and α-SMA staining, respectively (Figure 4C). The mRNA expression of *Col1a1* and *Acta2* were also reduced in *Yap1*-silenced tumors from HFD-fed mice compared with those in control tumors from HFD-fed mice (Figure 4D). The HA deposition increased by an HFD was significantly reduced by knockdown of *Yap1* (Figure 4, C and E). To prove the critical role of YAP activity in MC38 CRC cells for CAF activity, HSCs

were cocultured with control and *Yap1*-silenced MC38 cells. *Yap1* silencing in MC38 CRC cells significantly reduced the expression of *Has2* and *Col1a1* in HSCs compared with HSCs co-cultured with control MC38 cells (Figure 4F). These data suggest that YAP-mediated secreted factor(s) contribute to CAF activation. Because connective tissue growth factor (CTGF), encoded by *Ccn2,* and cysteine-rich angiogenic inducer 61 (CYR61) are secreted factors downstream of YAP signaling (Figure 4G), we investigated whether CTGF or CYR61 is responsible for CAF activation in liver metastasis. HSCs were treated with either CTGF or CYR61. Both CTGF and CYR61 increased *Col1a1* and *Timp1* mRNA expression (Supplemental Figure 4). However, only CTGF-treated HSCs showed increased *Has2* mRNA expression (Figure 4H and Supplemental Figure 4). To evaluate the effect of HA-mediated CTGF production from MC38 CRC cells on *Has2* expression in HSCs, HSCs were cocultured with control and *Ccn2*-silenced MC38 cells with or without LMW-HA treatment (Figure 4I). When MC38 cells were stimulated with LMW-HA, *Has2* mRNA expression levels were increased in HSCs. *Ccn2* knockdown in MC38 cells abolished this effect. Taken together, these results indicate that YAP signaling in cancer cells, enhanced by steatotic liver through HAS2-mediated HA production, feeds back to promote CAF activation, including HAS2 upregulation, to further increase the fibrotic TME (Figure 4J).

Increased CAF activity by steatotic liver contributes to a prometastatic immune TME

TAM M2 polarization is associated with a prometastatic immunosuppressive microenvironment in steatotic liver(13,14). As increased HAS2 expression by steatotic liver promotes metastatic

liver tumor growth, we investigated the impact of HAS2 on M2-TAM infiltration using *Has2*$^{\Delta HSC}$ mice. The increased infiltration of F4/80-positive and CD206-expressing M2-polarized TAMs by steatotic liver was decreased in mice with *Has2* deletion in HSCs (Figure 5, A-C). These results indicate CAF-derived HAS2 contributes to the infiltration of M2-polarized TAMs to metastatic lesions in steatotic liver. We further analyzed CAF and immune cell populations in the TME using single-cell RNA-seq. Unsupervised clustering identified 25 clusters, including 4 CAF, 2 M1, 4 M2, and 4 T cell clusters (Figure 5D, and Supplemental Figure 5, A-C). Although an HFD slightly decreased the proportion of CAF2, total CAF number was twice increased (Figure 5E, and 1F), and the CAF2 cluster increased the expression of HAS2 and CD44 with an HFD (Figure 5, E and F). These data underscore the number of total HAS2-expressing CAF2 cluster is increased in the steatotic liver. Furthermore, corroborated with the in vitro study showing cancer-derived YAP regulates HAS2 in HSCs (Figure 4F), silencing *Yap1* in cancer cells reduced *Has2* expression in the CAF2 cluster (Figure 5G). We then performed cell-cell interaction analysis between HAS2-expressing CAF2 and other immune cell clusters (Figure 5, H and I). CAF2 and macrophage/monocyte clusters show stronger interactions for an HFD than those for an LFD (Figure 5, H and I). Among macrophage subsets, the proportion of M2b-like cells was increased (Figure 5J). Because M2d-like cells expressed high levels of *Cd44* (Figure 5K), the ligand-receptor interaction between CAF2 and M2d-like cells could be mediated through HAS2-HA-CD44. Additionally, M2d cells highly expressed *Cd274* (which encodes programmed death-ligand 1 [PD-L1]), but *Cd274* expression was reduced when *Yap1* was silenced in cancer cells (Figure 5L). Although CAF3 expressed *Cd274*, the interactions between CAF3 and T cells were modest (Supplemental Figure 5, D-F). In contrast, increased interactions between M2d and T cells were observed in steatotic liver (Supplemental Figure 5, G and H); this could be due partly

to the increased expression of *Cd274* in M2d cells and *Pdcd1* (which encodes programmed cell death protein 1 [PD-1]) in T cells (Figure 5, K, M, and N). *Cd274* expression in M2d cells and *Pdcd1* expression in T cells were decreased when cancer *Yap1* was silenced (Figure 5, L and O). In summary, these findings suggest that cancer-derived YAP activity contributes to the HAS2-HA-CD44 interaction between CAFs and TAMs and the enhanced interaction of PD-L1 and PD-1 between TAMs and T cells (Figure 5P). These CAF-TAM-T cell interactions promote a prometastatic immunosuppressive TME in steatotic liver.

Increased myofibroblastic CAF infiltration is associated with immunosuppressive TAM and T cells in patients with CRC liver metastasis with steatotic liver

To translate our findings in mice to humans, we used tissue microarrays containing tissue specimens from 30 patients with CRC liver metastasis with and without steatotic liver (Supplemental Figure 6A)(14). First, we examined HA deposition. While almost no HA deposition was observed in nontumor liver tissues, tumors from patients with normal livers had high levels of HA deposition; the level of HA deposition in tumors was further increased in patients with steatotic liver (Figure 6, A and B). As we determined CTGF as an HA inducer (Figure 4), we assessed CTGF expression. CTGF levels were increased in tumors from patients with steatosis, and there is a significant correlation between HA and CTGF expression (Figure 6, A and C), corroborating our preclinical data. Then, we conducted imaging mass cytometry (IMC) using 42 metal-conjugated antibodies(14). We performed segmentation and phenotyping to identify liver-constituting and TME-constituting cell populations at the single-cell level, including hepatocytes, immune cells, CAFs, endothelial cells, and cancer cells (Figure 6D,

Supplemental Figure 6, B-D)(14). The numbers of total CAFs and myofibroblastic α-SMA-positive CAFs were increased in patients with MASLD (Figure 6D). Both CD44-positive and YAP-positive tumors had higher densities of α-SMA-positive and fibroblast activation protein (FAP)-positive CAFs than CD44-negative and YAP-negative tumors, respectively (Figure 6, E and F). The data suggest the α-SMA-positive CAF effect on CD44-positive tumors is mediated through HA, while YAP signaling actis on FAP-positive CAF recruitment. Also, CD44 and YAP expression was associated with the expression of PD-L1 and other immune checkpoint molecules in metastatic CRC cells (Figure 6, G and H), whereas PD-L1 expression was not associated with the distance and the density of CAFs near tumors (Supplemental Figure 6C). CAFs, TAMs, and T cells had higher CD44 expression than other cells (Supplemental Figure 6D). The expression of PD-L1, VISTA, and TIM3 was unchanged in CAFs between normal and MASLD livers (Supplemental Figure 6E). In contrast, the expression of PD-L1, VISTA, and TIM3 was higher in M2-TAMs and CD8 T cells of MASLD specimens, and CD8 T cells also had higher expression of PD-1 in MASLD specimens (Figure 6I, Supplemental Figure 6F). Of note, PD-L1 expression in M2-TAMs was positively associated with CD44 expression when M2-TAMs were close to CAFs as well as when the CAF density was high, suggesting the contribution of CAF-derived HA-CD44 signaling to PD-L1 expression in M2-TAMs (Figure 6, J and K). Taken together, these findings suggest that, in MASLD, CAF-derived HA acts on CD44-expressing TAMs and CRC cells to regulate PD-L1 expression; PD-L1 expression on M2-TAMs is associated with the distance and the density of CAFs near M2-TAMs; the increased PD-L1 binds to PD-1 expressed on CD8 T cells to support an immunosuppressive TME in metastatic foci in the presence of steatosis (Figure 6L).

Administration of 4-MU or 4-MUG inhibits the growth of metastatic cancer enhanced by steatotic liver

Last, we tested the potential of pharmacological inhibition of HA synthesis by 4-MU and 4-methylumbelliferyl glucuronide (4-MUG) to inhibit the growth of liver metastasis under the steatotic liver condition. C57BL/6 male WT mice were fed an LFD or an HFD diet and received a splenic injection of MC38 cells at the 6-week mark. We tested preventive and treatment interventions. For the prevention study, one group of mice received 450 mg/kg 4-MU orally and another group of mice received 2 mg/ml 4-MUG in their drinking water (Figure 7A). In LFD-fed mice, 4-MU and 4-MUG tended to reduce metastatic tumor growth, but it was not statistically significant (Figure 7, B and C). In HFD-fed mice, 4-MU and 4-MUG treatment significantly inhibited tumor growth, HA deposition (by HABP staining), collagen content (by Sirius red staining, mRNAs, and protein), and myofibroblastic CAFs (by α-SMA immunostaining, mRNA, and protein) (Figure 7, B-F, and Supplemental Figure 7, A-C). The 4-MU and 4-MUG treatment suppressed *Has1*, *Has2*, and *Has3* mRNA expression in HFD conditions (Figure 7G). We then examined YAP signaling. Phosphorylated YAP (pSer^{127}-YAP) has reduced transcriptional activity(26). We observed a significant reduction in pSer^{127}-YAP in tumors of HFD-fed mice compared with LFD-fed mice, along with a reciprocal increase in total YAP (Supplemental Figure 7D). When treated with 4-MU or 4-MUG in mice with HFD, there was an increased in pSer^{127}-YAP in the tumor, while total YAP decreased (Supplemental Figure 7D). Also, 4-MU or 4-MUG treatment downregulated YAP target genes, such as *Ccn1*, *Axl*, *Ankrd1*, and *Ccl2*, in steatotic liver tumors, mirroring the effects on *Yap1* mRNA expression (Supplemental Figure

7E). The increased presence of F4/80-positive TAMs in the tumors of HFD-fed mice was diminished by the inhibition of HA synthesis of 4-MU or 4-MUG (Supplemental Figure 7C). 4-MU or 4-MUG attenuated the expression of M2 macrophage-related markers and partially attenuated the expression of M1 macrophage markers (Supplemental Figure 7F). These results collectively indicate that 4-MU and 4-MUG treatment reduced the activity of YAP and its target genes, which contribute to suppressing metastatic tumor growth in MASLD. Additionally, we examined the efficacy of treatment regimen by starting the oral administration of 4-MU one week after tumor inoculation and continuing for an additional 3 weeks (Figure 7H). In the treatment regimen, we still observed the tumor suppression effect of 4-MU in the steatotic liver condition (Figure 7, I and J, Supplemental Figure 7G). 4-MU treatment reduced *Has2* mRNA, profibrogenic genes, and YAP target genes in the tumors of HFD-fed mice (Supplemental Figure 7H). HFD-fed mice exhibited reduced survival compared to LFD-fed mice, with a median survival of 29 days versus 41 days. Notably, 4-MU treatment extended survival in both LFD- and HFD-fed groups (Figure 7K). Lastly, we tested potential combination therapy of 4-MU and anti-PD-1 antibody. Anti-PD-1 therapy was effective in non-steatotic liver conditions, but it was ineffective in the steatotic liver (Figure 8). However, in combination with 4-MU, anti-PD-1 therapy showed the dramatic effect in suppressing metastatic liver tumor growth (Figure 8), suggesting the potential intervention of this combination.

Discussion

To date, MASLD is the leading cause of chronic liver disease and affects 30% of the population worldwide(27). The prognosis of MASLD is determined by its progression to metabolic dysfunction-associated steatohepatitis, fibrosis, cirrhosis, and the development of hepatocellular carcinoma(8,28). MASLD also increases the incidence of cardiovascular events(29) and cancers in extrahepatic organs, such as stomach, colon, pancreas, prostate, and breast(7,8). Liver is the most common metastasis site for CRC, and liver metastases substantially worsen CRC prognosis(1,2,5). We previously reported that steatotic hepatocyte-derived extracellular vesicles play pivotal roles in CRC liver metastasis by creating an immunosuppressive TME via YAP and CYR61(14). CYR61 is a regulator of M2 macrophage infiltration and polarization, which interacts with $PD1^{+}CD8T$ cells to create immunosuppressive TME. In the present study, we further explored a new mechanism of how MASLD promotes CRC liver metastasis. Here, we found that less desmoplastic CRC liver metastases become more desmoplastic when the liver is steatotic. Consistent with our previous report showing that HSCs are the responsible cells to produce HA through the upregulation of HAS2(20), HSC-derived CAFs actively produce HA through HAS2 upregulation in the steatotic liver. CAF-derived HA contributes to metastatic tumor growth mediated by YAP, likely through the CD44-FAK axis. Cancer-derived YAP conversely activates CAFs through the production of CTGF, a YAP downstream target. This bidirectional regulation between CAFs and cancer cells further promotes metastatic tumor growth. Our single-cell RNA-seq and IMC analyses further revealed that CAFs mediate PD-L1 upregulation in the nearest M2-TAMs, likely through the HA-CD44 interaction. Also, CD44-positivity and YAP-positivity affect PD-L1 expression and CAF density in metastatic CRC cells.

The upregulated PD-L1 in M2-TAMs and cancer cells further induces T cell exhaustion via PD-1. Last, we suggest that pharmacological HAS inhibition by 4-MU or 4-MUG, and combination therapy with anti-PD-1 antibody could be a treatment option for patients with CRC liver metastasis with MASLD. We summarized the underlying mechanisms reported previously and proposed here in Supplemental Figure 8.

Desmoplasia, which involves the deposition of fibrous ECM around a tumor, is observed frequently in pancreatic cancer and its liver metastases(30). The fibrous ECM deposition in CRC liver metastasis is variable(31). Increased fibrous ECM deposition is associated with poor prognosis and resistance to chemotherapies(30). Our data showed that steatotic liver enhanced ECM deposition and CAF myofibroblastic differentiation, which is further associated with the aggressiveness of metastatic tumor growth in the liver. FGF2 and PDGF have been implicated in promoting CRC metastasis. Elevated FGF2 levels have been shown to enhance tumor cell proliferation, angiogenesis, and migration, contributing to increased metastatic potential (32). Similarly, PDGF signaling in CRC and PDGF receptor signaling in CAFs promotes CRC metastasis(33,34). Our data showed that the expression of FGF2 and PDGF, growth factors known to activate HSCs(35), was elevated in the tumors under steatotic liver conditions (Figure 1E), suggesting their contribution to the fibrotic TME and metastatic niche formation. The contribution of the major ECM component, collagen, to tumor growth is complex. Intact collagens inhibit, whereas matrix metalloproteinase-degraded collagen promotes pancreatic cancer growth(30). Similarly, HA comprises different sizes that have opposing biological activities(20,21). HAS2 controls HA synthesis in HSCs, and HAS2-derived HA promotes fibrosis progression and cancer aggressiveness in breast, esophageal, bile duct, pancreatic, and

other cancers(17,18,20,36-38). Our data demonstrated that HAS2 expressed in HSC-derived CAFs contributes to HA production and promotes the growth of CRC liver metastasis under the steatotic liver condition. Other HAS isoenzymes, such as HAS1 or HAS3, could also contribute to HA deposition because HA still remained detectable in HAS2 null mice. HAS1 and HAS3 expression are indeed increased in metastatic tumors of HFD-fed mice compared to LFD-fed mice. However, HAS2 shows the most pronounced upregulation among the three enzymes. It is likely that HAS1 and HAS3 act cooperatively with HAS2 to support HA deposition and tumor growth. Nonetheless, our data suggested that HAS2 plays the dominant role in MASLD-associated liver metastasis. HAS2 primarily synthesizes HA as HMW forms, and HA is then degraded into LMW-HA by hyaluronidases, including hyaluronidase 1 to 4 and cell surface hyaluronidase (CEMIP2, also known as TMEM2). HMW-HA and LMW-HA have different biological effects(20,21,23). HMW-HA has anti-inflammatory and anti-proliferative properties, whereas LMW-HA promotes cell migration, proliferation, and immune cell influx(39). Our study revealed that LMW-HA is pro-cancerous, and LMW-HA is the dominant form in the serum and tumor of steatotic livers. The precise mechanism that converts HA from HMW to LMW forms in CAFs and cancers remains unknown. TMEM2 is a candidate for this process, as its levels were found to be elevated in metastatic tumors of HFD-fed mice (Figure 1E); however, further investigation is required.

In addition to MASLD, other liver diseases, including alcohol-associated liver disease (ALD), hepatitis B, and cirrhosis in humans, and ALD and carbon tetrachloride-induced liver injury in mice(40-43), also enhance liver metastasis growth. In our previous and present studies, we determined EV production and ECM deposition are mechanisms of enhanced liver metastasis

in MASLD. Additional factors, including lipid metabolism, inflammatory signaling, and immune cells, are also involved in this process(44,45). Further research is needed to determine whether other mechanisms are involved in promoting liver metastasis in MASLD and other liver disease.

The primary receptors for HA are CD44 and Toll-like receptor 4(20,23). CD44 is a cancer stem cell marker and has a cell-adhesive capacity for interaction with cancer cells. Our data demonstrated that CD44 expression was elevated in cancer cells under steatotic liver conditions and was closely associated with the nearest CAF density that may amplify the HA-mediated signaling pathway to enhance the proliferation, invasion, and metastasis of CRC cells in the liver. CD44 is also expressed in myeloid and lymphoid cells. Our single-cell analysis revealed that steatotic liver promoted CD44 and PD-L1 expression in M2-TAM and cancer cells, which was associated with the nearest CAF distance and density. This suggests that CAF-derived HA interacts with the nearest M2-TAMs and cancer cells through CD44, promoting the upregulation of PD-L1 together with PD-1-expressing T cells to create a protumorigenic immunosuppressive TME in steatotic liver.

Hippo-YAP signaling is a pivotal protumorigenic and prometastatic factor in many cancers through interaction with the transcriptional enhanced associate domain (TEAD) transcription factors(25,46-48). YAP regulates tumor growth and progression both intrinsically and extrinsically. YAP signaling promotes cancer cell growth and survival, which is in line with our findings that YAP silencing in cancer cells diminishes tumor growth in non-steatotic livers (Figure 4A). Simultaneously, YAP senses changes in the external environment and responds to the signals. In MASLD, CAF-derived HAS2 and LMW-HA augmented YAP nuclear translocation and YAP downstream gene expression. FAK is responsible for LMW-HA-induced

YAP nuclear translocation. YAP not only acts downstream of the HA-CD44 signaling pathway but also plays a role in the activation of CAFs by producing CTGF (Figure 5P). Indeed, liver metastases by YAP-silencing CRC cells had reduced CAF activity, collagen and HA deposition, and CTGF expression. In HSCs, CTGF upregulates HAS2 expression. Additionally, our IMC data suggested that CD44 and YAP reciprocally regulate in cancer cells and that CD44 and YAP expression are associated with PD-L1 expression and CAF density in cancer regions. These data collectively suggest bidirectional regulation between CAFs and cancer cells through HAS2-HA-CD44-YAP signaling. Further study could identify more precise molecular mechanisms of the bidirectional regulation between CAFs and cancer cells in CRC liver metastasis.

Because our study revealed the procarcinogenic and prometastatic role of HAS2 and HA, modulation of HAS2 and HA production can be a therapeutic strategy to inhibit metastatic tumor growth in steatotic liver. Also, ECM deposition prevents the delivery of anticancer drugs to cancer lesions. Therefore, reduction of ECM deposition may enhance the efficacy of other anticancer drugs. However, clinical trials for pancreatic cancer using a hyaluronidase PEGPH20 to promote the reduction of HA deposition did not show a favorable result.(49) This could be explained by the fact that PEGPH20 degrades HA to generate protumorigenic LMW-HA. In contrast, the approach that we tested in this study is that we inhibited HA synthesis by the HAS synthase inhibitors 4-MU and 4-MUG. We previously reported that 4-MU inhibits HA synthesis and liver fibrosis progression.(20,50) Our present study showed that 4-MU or 4-MUG treatment inhibited the expression of all three HAS enzymes, HA synthesis, CAF activity, and M2 macrophage infiltration (Figure 7). Hepatic macrophages and TAMs polarize into M2 macrophages in metastatic tumors.(13,14) An increase in M2 macrophages is associated with

poor prognosis of patients with CRC liver metastasis.(51) We also demonstrated the importance of M2-TAM polarization in metastatic liver tumor growth in MASLD.(13,14) Together with our data in the present study, these findings underscore that inhibition of HA synthesis suppresses tumor growth in steatotic liver by suppressing HA deposition, CAF activation, and M2-TAM infiltration. We expect that, unlike PEGPH20, our approach would not lead to the detrimental effect. In addition, although anti-PD-1 therapy is ineffective in steatotic livers, we found combination therapy of 4-MU and anti-PD-1 antibody effectively suppressed metastatic tumor growth even in steatotic liver conditions. The combination therapy can be a potential therapy for patients with MASLD and liver metastasis.

In summary, steatotic liver is associated with an enhanced fibrotic TME, comprising myofibroblastic CAFs and HA deposition, that contributes to metastatic tumor growth. Additionally, the cancer cell activity enhanced by CAFs and HA further creates a feed-forward loop to promote CAF activity, ECM production, and an immunosuppressive TME under steatotic liver conditions. The underlying molecular mechanisms of metastatic tumor growth may differ in normal and steatotic liver conditions. As the number of patients with cancer with basal steatotic liver is increasing, understanding the precise molecular mechanism of metastatic tumor growth in both normal and MASLD liver could help provide more appropriate clinical management for those patients. Although underlying chronic liver disease may inhibit the efficacy of anticancer therapies, including anti-PD-1 therapy, 4-MU and 4-MUG have the potential to suppress steatotic liver-associated metastatic tumor growth. The pharmacological inhibition of HA synthesis can be considered as an option to treat patients with metastatic cancer with steatotic liver.

Methods

Sex as a biological variable

Sex was not considered as a biological variable.

Cell line

MC38 mouse CRC cells were a gift from Dr. Michael Karin(14). CMT93 mouse CRC cells were obtained from the American Type Culture Collection (ATCC). Pan02 mouse pancreatic cancer cells were a gift from Dr. Robert Schwabe(18). Cells were cultivated in normal Dulbecco's modified Eagle medium (DMEM) without pyruvate (MC38 and CMT93) or RPMI-1640 (Pan02), supplemented with 10% fetal bovine serum (FBS), and 1% penicillin/streptomycin at 37℃ in a humidified 5% CO_2 incubator. Before use, FBS underwent heat inactivation. Mycoplasma contamination was checked, and cell line authenticity was confirmed through authentication by the American Type Culture Collection (ATCC). Previously, stably transfected MC38 cells expressing either shCon (control) or sh*Yap1* (Yap1 knockdown) were established via puromycin selection(14).

Mice

Seven-week-old C57BL/6 male mice were purchased from Jackson Laboratories or KOATECH Inc. *Lrat*-Cre Tg mice expressing TdTomato were generously provided by Dr. Robert Schwabe

(Columbia University). Our study examined male mice because male animals exhibited less variability in the phenotype of hepatic steatosis. To generate HSC-specific *Has2* knockout mice, *Lrat*-Cre Tg and *Has2*$^{fl/fl}$ mice were crossed, as previously described(20,22). Genetically modified mice underwent at least 10 generations of back-crossing onto the C57BL/6 background. Upon reaching 8 weeks of age, mice were randomly assigned to either a low-fat diet (LFD, PicoLab® Rodent Diet 20, Cat# 5053) or a high-fat diet containing 60% of calories from fat (HFD, Research Diets, Cat# D12492 or Bio-Serv, Cat# S3282). The mice underwent an 8-week dietary intervention period. Food intake and body weight were measured weekly. Mice were housed in the same specific pathogen-free conditions within the animal facility at Cedars-Sinai Medical Center or at Kangwon National University Animal Laboratory Center. All animal studies adhered to the National Institutes of Health recommendations as delineated in the Guide for the Care and Use of Laboratory Animals.

Human specimens

Patients' biospecimens were obtained from those diagnosed with CRC liver metastasis and coexisting MASLD, and subjects with normal livers undergoing surgical resection or tissue biopsy at Cedars-Sinai Medical Center(14). Comprehensive clinical, demographic, and pathologic data were retrospectively extracted from electronic medical records for subsequent analysis (Supplemental Table 1)(14). A tissue microarray block was created using primary CRC, CRC liver metastasis, and adjacent non-cancer liver tissues from 17 patients without MASLD and 13 patients with MASLD as previously described and applied for IMC and staining(14).

Liver metastasis splenic injection in vivo model

A murine model of liver metastasis was established splenic injection of MC38, CMT93, and Pan02 cells, as previously described(13,14,52). In brief, trypsinized MC38, CMT93, and Pan02 cells were resuspended in cold phosphate-buffered saline (PBS). The mice, having fed either LFD or HFD feeding, were subjected to anesthesia. Following a laparotomy, MC38 cells (2×10^4 or 2×10^5 cells), MC38 cells stably expressing either shCon or sh*Yap1* (1×10^5 cells), CMT93 (1×10^6 cells), and Pan02 (1×10^6 cells) were injected into the spleen. Spleen was removed, and the abdomen was closed. After two weeks of CRC cell inoculation, mice were euthanized for subsequent analysis and sampling. For the prevention study with HA synthesis inhibitors, mice were divided into 6 groups: LFD-Vehicle (n=8), LFD-4-methylumbelliferone (4-MU) (n=6), LFD-4-methylumbelliferyl-β-D(-)-glucuronide (4-MUG) (n=8), HFD-Vehicle (n=8), HFD-4-MU (n=9), and HFD-4-MUG (n=9). 450 mg/kg of 4-MU (Sigma-Aldrich, Cat# M1508) or vehicle control (2% sucrose) was orally administered daily at 450 mg/kg and 4-MUG (Chem-Impex, Cat# 20981) was administered to mice via drinking water at a final concentration of 2 mg/ml, starting two weeks before the injection of cancer cells and continued until the point of sacrifice. For the treatment study, mice were treated with 4-MU (orally administered at 450 mg/kg daily), starting one week after tumor inoculations (2×10^4 MC38 cells) and continued for an additional three weeks. For the survival study, mice were treated with 4-MU (orally administered at 450 mg/kg daily), starting one week after tumor inoculations (2×10^4 MC38 cells) and continuing until death. For the combination therapy, mice were treated with 4-MU (orally administered at 450 mg/kg daily) and anti-PD-1 antibody (BioXCell, Cat#BP0146; 200 μg intraperitoneally every three days) or control

IgG (BioXCell, Cat#BP0089) one day after MC38 cell (2×10^5 cells) inoculation and continued for an additional two weeks.

Statistics

Statistical significance was confirmed by GraphPad Prism 8 (GraphPad Software Inc. Statistical significance between the two groups was compared by two-tailed unpaired Student *t* test. Comparisons between different groups were performed using one-way ANOVA test, followed by Tukey's *post hoc* analysis. Correlation analysis was performed using the Pearson correlation coefficient. Survival curves were generated using the Kaplan-Meier method and compared using the log-rank test. A *P* value less than 0.05 was considered significant.

Study approval

Samples from patients with CRC liver metastasis were analyzed. The study was approved by the Cedars-Sinai Medical Center Institutional Review Board (IRB No. 0901). Written informed consent was obtained from all participants. All animal experiments were approved by the Cedars-Sinai Medical Center Institutional Animal Care and Use Committee (IACUC No. 8412) and the Kangwon National University Animal Protection and Use Committee (IACUC No. KW-200225-1 and KW-240620-1).

Data Availability

RNA-seq data of the liver metastatic tumor tissue in HFD-fed and LFD-fed mice and gene expression profile at single cell level of immune cells from the liver metastasized tumor tissue were previously deposited in gene expression omnibus (GSE227913 and GSE227914). All supporting data are provided in the Supporting Data Values file.

Author contributions

Designing research studies, E.S., Y.M.Y., S.Y.Y., and A.M.X.; Conducting experiments, Y.M.Y., Z.W., S.Y.K., Jieun K., G.J.C., J.H.L., S.M.K., A.M.X., A.M., S.Y.Y., and Jina K.; Acquiring data, Y.M.Y., Z.W., Jieun K., S.Y.K., G.J.C., J.H.L., S.M.K., T.T., and M.M.; Analyzing data, Y.M.Y., Z.W., S.Y.K., Jieun K., G.J.C., A.M.X., Jina K., S.Y.Y., and E.S.; Writing – Original Draft, E.S. and Y.M.Y.; Writing – Review & Editing, Y.M.Y., A.M.X., Jieun K., V.P., S.P., N.B., S.Y.Y., S.C.L., E.S., and; Funding acquisition, E.S., E.P., N.B., S.C.L., J.K., and Y.M.Y.; Resources, A.G., M.S.L., A.M., P.W.N., D.J., and E.P.; Supervision, E.S. The order in which the co-first authors are listed was determined by the order of their entry into the study.

Acknowledgements

This work is supported by the National Institutes of Health (P01CA233452 to E.S., N.B., S.P., E.P., S.Y.Y., and S.C.L.; R21AA025841 to E.S. and S.C.L.; R01DK085252 and R01DK138591 to E.S.), NIH National Center for Advancing Translational Science (NCATS) UCLA CTSI (UL1TR001881 to A.M.X.), the Center for Integrated Research in Cancer and Lifestyle Award, and a Project Acceleration Award by the Cedars-Sinai Cancer Center at Cedars-Sinai Medical

Center (to E.S. and S.P.), grants from the National Research Foundation of Korea (RS-2023-00301850, RS-2023-00210489, and RS-2024-00441114 to Y.M.Y.), and American Liver Foundation Postdoctoral Fellowship (to J.K.). The authors acknowledge the Spatial Molecular Profiling Shared Resource (SMPSR), the Applied Genomics Shared Resource (AGSR), Biomedical Data Shared Resource (BDSSR), and OncoBiobank Shared Resource (OBSR) at Cedars-Sinai Medical Center and Cedars-Sinai Cancer. Special thanks to Ms. Fiona Miao and Ms. Rie Seki (Department of Medicine at Cedars-Sinai Medical Center) for their technical assistance. The illustrations were created with BioRender.com

References

1. Tsilimigras DI, Brodt P, Clavien PA, Muschel RJ, D'Angelica MI, Endo I, et al. Liver metastases. *Nat Rev Dis Primers.* 2021;7(1):27.
2. Siegel RL, Wagle NS, Cercek A, Smith RA, and Jemal A. Colorectal cancer statistics, 2023. *CA Cancer J Clin.* 2023;73(3):233-54.
3. Patel RK, Rahman S, Schwantes IR, Bartlett A, Eil R, Farsad K, et al. Updated Management of Colorectal Cancer Liver Metastases: Scientific Advances Driving Modern Therapeutic Innovations. *Cell Mol Gastroenterol Hepatol.* 2023;16(6):881-94.
4. Wang CB, Shahjehan F, Merchea A, Li Z, Bekaii-Saab TS, Grothey A, et al. Impact of Tumor Location and Variables Associated With Overall Survival in Patients With Colorectal Cancer: A Mayo Clinic Colon and Rectal Cancer Registry Study. *Front Oncol.* 2019;9:76.
5. Zhou H, Liu Z, Wang Y, Wen X, Amador EH, Yuan L, et al. Colorectal liver metastasis: molecular mechanism and interventional therapy. *Signal Transduct Target Ther.* 2022;7(1):70.
6. Calle EE, Rodriguez C, Walker-Thurmond K, and Thun MJ. Overweight, obesity, and mortality from cancer in a prospectively studied cohort of U.S. adults. *N Engl J Med.* 2003;348(17):1625-38.
7. Kim GA, Lee HC, Choe J, Kim MJ, Lee MJ, Chang HS, et al. Association between non-alcoholic fatty liver disease and cancer incidence rate. *J Hepatol.* 2017.
8. Allen AM, Hicks SB, Mara KC, Larson JJ, and Therneau TM. The risk of incident extrahepatic cancers is higher in non-alcoholic fatty liver disease than obesity - A longitudinal cohort study. *J Hepatol.* 2019;71(6):1229-36.
9. Hamady ZZ, Rees M, Welsh FK, Toogood GJ, Prasad KR, John TK, et al. Fatty liver disease as a predictor of local recurrence following resection of colorectal liver metastases. *Br J Surg.* 2013;100(6):820-6.
10. Wu K, Zhai MZ, Weltzien EK, Cespedes Feliciano EM, Meyerhardt JA, Giovannucci E, et al. Non-alcoholic fatty liver disease and colorectal cancer survival. *Cancer Causes Control.* 2019;30(2):165-8.
11. Yang S, Peng R, and Zhou L. The impact of hepatic steatosis on outcomes of colorectal cancer patients with liver metastases: A systematic review and meta-analysis. *Front Med (Lausanne).* 2022;9:938718.
12. Lv Y, and Zhang HJ. Effect of Non-alcoholic Fatty Liver Disease on the Risk of Synchronous Liver Metastasis: Analysis of 451 Consecutive Patients of Newly Diagnosed Colorectal Cancer. *Front Oncol.* 2020;10:251.
13. Ohashi K, Wang Z, Yang YM, Billet S, Tu W, Pimienta M, et al. NOD-like receptor C4 Inflammasome Regulates the Growth of Colon Cancer Liver Metastasis in NAFLD. *Hepatology.* 2019;70(5):1582-99.
14. Wang Z, Kim SY, Tu W, Kim J, Xu A, Yang YM, et al. Extracellular vesicles in fatty liver promote a metastatic tumor microenvironment. *Cell Metab.* 2023;35(7):1209-26 e13.
15. Wang Y, Tu K, Liu D, Guo L, Chen Y, Li Q, et al. p300 Acetyltransferase Is a Cytoplasm-to-Nucleus Shuttle for SMAD2/3 and TAZ Nuclear Transport in Transforming Growth Factor beta-Stimulated Hepatic Stellate Cells. *Hepatology.* 2019;70(4):1409-23.
16. Dou C, Liu Z, Tu K, Zhang H, Chen C, Yaqoob U, et al. P300 Acetyltransferase Mediates Stiffness-Induced Activation of Hepatic Stellate Cells Into Tumor-Promoting Myofibroblasts. *Gastroenterology.* 2018;154(8):2209-21 e14.

17. Affo S, Nair A, Brundu F, Ravichandra A, Bhattacharjee S, Matsuda M, et al. Promotion of cholangiocarcinoma growth by diverse cancer-associated fibroblast subpopulations. *Cancer Cell.* 2021;39(6):866-82 e11.
18. Bhattacharjee S, Hamberger F, Ravichandra A, Miller M, Nair A, Affo S, et al. Tumor restriction by type I collagen opposes tumor-promoting effects of cancer-associated fibroblasts. *J Clin Invest.* 2021;131(11).
19. Filliol A, Saito Y, Nair A, Dapito DH, Yu LX, Ravichandra A, et al. Opposing roles of hepatic stellate cell subpopulations in hepatocarcinogenesis. *Nature.* 2022;610(7931):356-65.
20. Yang YM, Noureddin M, Liu C, Ohashi K, Kim SY, Ramnath D, et al. Hyaluronan synthase 2-mediated hyaluronan production mediates Notch1 activation and liver fibrosis. *Sci Transl Med.* 2019;11(496).
21. Ooki T, Murata-Kamiya N, Takahashi-Kanemitsu A, Wu W, and Hatakeyama M. High-Molecular-Weight Hyaluronan Is a Hippo Pathway Ligand Directing Cell Density-Dependent Growth Inhibition via PAR1b. *Dev Cell.* 2019;49(4):590-604 e9.
22. Mederacke I, Hsu CC, Troeger JS, Huebener P, Mu X, Dapito DH, et al. Fate tracing reveals hepatic stellate cells as dominant contributors to liver fibrosis independent of its aetiology. *Nat Commun.* 2013;4:2823.
23. Kim J, and Seki E. Hyaluronan in liver fibrosis: basic mechanisms, clinical implications, and therapeutic targets. *Hepatol Commun.* 2023;7(4).
24. Song X, Xu H, Wang P, Wang J, Affo S, Wang H, et al. Focal adhesion kinase (FAK) promotes cholangiocarcinoma development and progression via YAP activation. *J Hepatol.* 2021;75(4):888-99.
25. Moroishi T, Hansen CG, and Guan KL. The emerging roles of YAP and TAZ in cancer. *Nat Rev Cancer.* 2015;15(2):73-9.
26. Kim W, Khan SK, Gvozdenovic-Jeremic J, Kim Y, Dahlman J, Kim H, et al. Hippo signaling interactions with Wnt/beta-catenin and Notch signaling repress liver tumorigenesis. *J Clin Invest.* 2017;127(1):137-52.
27. Malhi H, Brown RS, Jr., Lim JK, Reau N, Tapper EB, Wong CC, et al. Precipitous changes in nomenclature and definitions-NAFLD becomes SLD: Implications for and expectations of AASLD journals. *Hepatology.* 2023;78(6):1680-1.
28. Tsuchida T, and Friedman SL. Mechanisms of hepatic stellate cell activation. *Nat Rev Gastroenterol Hepatol.* 2017;14(7):397-411.
29. Xiao J, Ng CH, Chan KE, Fu C, Tay P, Yong JN, et al. Hepatic, Extra-hepatic Outcomes and Causes of Mortality in NAFLD - An Umbrella Overview of Systematic Review of Meta-Analysis. *J Clin Exp Hepatol.* 2023;13(4):656-65.
30. Su H, Yang F, Fu R, Trinh B, Sun N, Liu J, et al. Collagenolysis-dependent DDR1 signalling dictates pancreatic cancer outcome. *Nature.* 2022;610(7931):366-72.
31. Ao T, Kajiwara Y, Yonemura K, Shinto E, Mochizuki S, Okamoto K, et al. Prognostic significance of histological categorization of desmoplastic reaction in colorectal liver metastases. *Virchows Arch.* 2019;475(3):341-8.
32. Razavi ZS, Asgarpour K, Mahjoubin-Tehran M, Rasouli S, Khan H, Shahrzad MK, et al. Angiogenesis-related non-coding RNAs and gastrointestinal cancer. *Mol Ther Oncolytics.* 2021;21:220-41.
33. Jiang B, Chen J, Yuan W, Ji J, Liu Z, Wu L, et al. Platelet-derived growth factor-D promotes colorectal cancer cell migration, invasion and proliferation by regulating Notch1 and

matrix metalloproteinase-9. *Oncol Lett.* 2018;15(2):1573-9.

34. Pena C, Cespedes MV, Lindh MB, Kiflemariam S, Mezheyeuski A, Edqvist PH, et al. STC1 expression by cancer-associated fibroblasts drives metastasis of colorectal cancer. *Cancer Res.* 2013;73(4):1287-97.

35. Qi M, Fan S, Huang M, Pan J, Li Y, Miao Q, et al. Targeting FAPalpha-expressing hepatic stellate cells overcomes resistance to antiangiogenics in colorectal cancer liver metastasis models. *J Clin Invest.* 2022;132(19).

36. Passi A, Vigetti D, Buraschi S, and Iozzo RV. Dissecting the role of hyaluronan synthases in the tumor microenvironment. *FEBS J.* 2019;286(15):2937-49.

37. Bernert B, Porsch H, and Heldin P. Hyaluronan synthase 2 (HAS2) promotes breast cancer cell invasion by suppression of tissue metalloproteinase inhibitor 1 (TIMP-1). *J Biol Chem.* 2011;286(49):42349-59.

38. Kretschmer I, Freudenberger T, Twarock S, Yamaguchi Y, Grandoch M, and Fischer JW. Esophageal Squamous Cell Carcinoma Cells Modulate Chemokine Expression and Hyaluronan Synthesis in Fibroblasts. *J Biol Chem.* 2016;291(8):4091-106.

39. Liu M, Tolg C, and Turley E. Dissecting the Dual Nature of Hyaluronan in the Tumor Microenvironment. *Front Immunol.* 2019;10:947.

40. Im HJ, Kim HG, Lee JS, Kim HS, Cho JH, Jo IJ, et al. A Preclinical Model of Chronic Alcohol Consumption Reveals Increased Metastatic Seeding of Colon Cancer Cells in the Liver. *Cancer Res.* 2016;76(7):1698-704.

41. Mohr AM, Gould JJ, Kubik JL, Talmon GA, Casey CA, Thomas P, et al. Enhanced colorectal cancer metastases in the alcohol-injured liver. *Clin Exp Metastasis.* 2017;34(2):171-84.

42. Qiu X, Zhou J, Xu H, Li Y, Ma S, Qiao H, et al. Alcohol reshapes a liver premetastatic niche for cancer by extra- and intrahepatic crosstalk-mediated immune evasion. *Mol Ther.* 2023;31(9):2662-80.

43. Wei X, Wang L, Yang B, Ma Y, Yuan W, and Ma J. Orosomucoid 2 upregulation mediates liver injury-induced colorectal cancer liver metastasis by promoting EMT and cell migration. *Cancer Sci.* 2024.

44. Kim J, and Seki E. Unveiling the cancer risk nexus of the steatotic liver. *Trends Endocrinol Metab.* 2024;35(8):708-19.

45. Kim J, and Seki E. Inflammation and Immunity in Liver Neoplasms: Implications for Future Therapeutic Strategies. *Mol Cancer Ther.* 2024.

46. Overholtzer M, Zhang J, Smolen GA, Muir B, Li W, Sgroi DC, et al. Transforming properties of YAP, a candidate oncogene on the chromosome 11q22 amplicon. *Proc Natl Acad Sci U S A.* 2006;103(33):12405-10.

47. Wang X, Su L, and Ou Q. Yes-associated protein promotes tumour development in luminal epithelial derived breast cancer. *Eur J Cancer.* 2012;48(8):1227-34.

48. Harvey KF, Zhang X, and Thomas DM. The Hippo pathway and human cancer. *Nat Rev Cancer.* 2013;13(4):246-57.

49. Van Cutsem E, Tempero MA, Sigal D, Oh DY, Fazio N, Macarulla T, et al. Randomized Phase III Trial of Pegvorhyaluronidase Alfa With Nab-Paclitaxel Plus Gemcitabine for Patients With Hyaluronan-High Metastatic Pancreatic Adenocarcinoma. *J Clin Oncol.* 2020;38(27):3185-94.

50. Yang YM, Wang Z, Matsuda M, and Seki E. Inhibition of hyaluronan synthesis by 4-methylumbelliferone ameliorates non-alcoholic steatohepatitis in choline-deficient L-amino acid-

defined diet-induced murine model. *Arch Pharm Res.* 2021;44(2):230-40.

51. Donadon M, Torzilli G, Cortese N, Soldani C, Di Tommaso L, Franceschini B, et al. Macrophage morphology correlates with single-cell diversity and prognosis in colorectal liver metastasis. *J Exp Med.* 2020;217(11).

52. VanSaun MN, Lee IK, Washington MK, Matrisian L, and Gorden DL. High fat diet induced hepatic steatosis establishes a permissive microenvironment for colorectal metastases and promotes primary dysplasia in a murine model. *Am J Pathol.* 2009;175(1):355-64.

Figure legends

Figure 1. High-fat diet-induced steatotic liver increases HA accumulation and HAS2 expression in tumors.
(A) Representation of the mouse model illustrating the induction of steatotic liver and subsequent splenic injection of MC38 cells to form liver metastases. LFD, low-fat diet; HFD, high-fat diet. **(B)** Macroscopic appearance of the liver with arrows indicating tumor sites. Scale bar: 1 cm. **(C)** Representative images of hematoxylin and eosin (H&E)-stained tumor and quantitative assessment of tumor area based on H&E staining. (n = 4-5 per group) Scale bar: 500 μm. **(D)** RNA-seq analysis. Gene set enrichment analysis (GSEA) of gene expression for extracellular matrix (ECM) and liver fibrosis in tumors from mice fed an LFD or an HFD (upper). Enrichment plot for ECM organization (lower). FDR, false discovery rate; NES, normalized enrichment score. NOM, nominal. **(E)** A heat map of the hyaluronic acid (HA)-related genes. (n = 5) **(F)** Representative microscopic images depicting liver sections stained for alpha-smooth muscle actin (α-SMA), with Sirius red, and for hyaluronic acid binding protein (HABP). Scale bars: 200 μm. Quantification of α-SMA-positive area, Sirius red-positive area, and HABP-positive area. (n = 4-5 per group) **(G)** Comparison of mRNA expression levels of *Has2* in nontumor (NT) and tumor tissues from mice fed an LFD or an HFD. (n = 8 per group) **(H)** Representative images of RNAscope *in situ* hybridization for *Has2*. Data are presented as mean ± SEM. Statistical significance was calculated with Student t-test (C, F) and one-way analysis of variance followed by Tukey post hoc test (G). P values are indicated ($^{*}P < 0.05$ or $^{**}P < 0.01$).

Figure 2. Suppression of metastatic liver tumor growth enhanced by metabolic dysfunction-associated steatotic liver disease through HSC-specific *Has2* deficiency.

(A) Macroscopic appearance of the liver. Wild-type (WT) and $Has2^{\Delta HSC}$ mice were intrasplenically injected with MC38 cells after 6 weeks of either low-fat diet (LFD) or high-fat diet (HFD) feeding. Mice were maintained on their respective diets for an additional 2 weeks. Arrows indicate the tumors. Scale bar: 1 cm. **(B)** Measurement of liver weight, maximal tumor diameter, and number of nodules. (n = 10-12 per group) KO, knockout. **(C)** Representative images of hematoxylin and eosin (H&E) staining of liver tissue sections. Scale bar: 200 μm. **(D)** Representative images and quantification of hyaluronic acid binding protein (HABP) staining. (n = 6) Scale bar: 200 μm. **(E)** Representative images and quantification of alpha-smooth muscle actin (α-SMA) and Sirius red staining of liver tissue sections. (n = 6) Scale bar: 200 μm. Data are presented as mean ± SEM. Statistical significance was calculated with one-way analysis of variance followed by Tukey post hoc test. P values are indicated ($^{*}P < 0.05$ or $^{**}P < 0.01$).

Figure 3. HAS2 and low molecular weight HA play an important role in cancer cell aggressiveness and YAP activation.

(A) Serum hyaluronic acid (HA) levels (left) and tumor HA levels (right) between tumor-bearing mice on a low-fat diet (LFD) and those on a high-fat diet (HFD). (serum, n = 5-6 per group; tumor, n = 8 per group) **(B)** Fractionated analysis of HA content, distinguishing between high-molecular weight (HMW)-HA (>300 kDa), medium molecular weight (MMW)-HA (100~300 kDa), and low-molecular weight (LMW)-HA (<100 kDa). Serum and tissue homogenate samples from HFD-fed, tumor-bearing mice were fractionated using columns. (serum, n = 4; tumor, n = 8) **(C)** The influence of LMW-HA and HMW-HA on the colony formation and **(D)** invasion ability of MC38 cells. (n = 3) **(E)** The effect of LMW-HA and HMW-HA on *Yap1* and *Ccn2* mRNA expression in MC38 cells. (n = 3) Con, control. **(F)** The correlation between LMW-HA levels and *Ccn2* mRNA expression in tumors from mice on an LFD and an HFD. The Pearson correlation coefficient (r) was calculated. (n = 5) **(G)** Effect of hepatic stellate cell (HSC)-specific *Has2* deletion on YAP expression in tumors from wild-type (WT) mice or knockout (KO) mice. (n = 8) Representative images of YAP staining were shown. NT, nontumor; T, tumor. Scale bar: 100 μm. **(H)** The effect of *Yap1* knockdown in MC38 cells on LMW-HA-induced cancer cell invasion. The number of invaded cells per field is shown. (n = 3) Sh, short hairpin. Data are presented as mean ± SEM. Statistical significance was calculated with Student t-test (A, H) and one-way analysis of variance followed by Tukey post hoc test (B-E). P values are indicated ($^{*}P < 0.05$ or $^{**}P < 0.01$).

Figure 4. YAP knockdown attenuates colorectal cancer aggressiveness and cancer-associated fibroblast activation.

(A) Following six weeks of low-fat diet (LFD) or high-fat diet (HFD) feeding, MC38 cells with either shCon or sh*Yap1* were intrasplenically injected into mice. Liver weight (left), maximum tumor size (middle), and number of nodules (right) (n = 7-8 per group) **(B)** Gene set enrichment analysis. NES, normalized enrichment score. NOM, nominal. **(C)** Representative Sirius red (upper), α-SMA (middle), and hyaluronic acid binding protein (HABP) (lower) in metastatic liver tumors. **(D)** mRNA expression of *Col1a1* and *Acta2* in tumor tissues. (n = 8) **(E)** Quantification of HABP-positive area. (n = 5-6 per group) **(F)** Co-culture experiments. *Has2* and *Col1a1* mRNA levels in mouse primary hepatic stellate cells (HSCs) ShCon-MC38 or sh*Yap1*-MC38 cells were placed in the upper chamber and primary HSCs were seeded in the lower chamber. (n = 3) **(G)** *Ccn2* mRNA levels in tumor tissues. (n = 8) **(H)** CTGF treatment in primary HSCs. (n = 3) **(I)** *Has2* mRNA levels in mouse primary HSCs. MC38 cells were transiently transfected with siCon or si*Ccn2* and treated with vehicle or LMW-HA. MC38 cells were loaded in the upper chamber. HSCs were seeded in the lower chamber one day before coculture. Coculture lasted 48 hours. (n = 4) **(J)** Illustration showing the bidirectional regulation between HSC and CRC. Data are presented as mean ± SEM. Statistical significance was calculated with Student t-test (D, F, G, H) and one-way analysis of variance followed by Tukey post hoc test (A, E, I). P values are indicated (*$P < 0.05$ or **$P < 0.01$).

Figure 5. CAF-derived HAS2 and cancer-derived YAP contribute to a prometastatic immune tumor microenvironment in steatotic liver.

(A,B) Representative immunohistochemistry images for (A) F4/80 and (B) CD206 from tumors in Figure 2. HFD, high-fat diet; HSC, hepatic stellate cell; LFD, low-fat diet; WT, wild-type. Scale bar: 200 μm. **(C)** Quantification of F4/80-positive (upper) and CD206-positive (lower) areas. (*n* = 5-7 per group) KO, knockout. Data are presented as mean ± SEM. Statistical significance was calculated with one-way analysis of variance followed by Tukey post hoc test. **(D)** Tumor-infiltrating cancer-associated fibroblast (CAF) and immune cell populations. Uniform manifold approximation and projection (UMAP) of single-cell RNA-seq from 46,577 cells showing 25 clusters determined by integrated analysis, colored by cluster. Cells were from metastatic liver tumors of LFD-fed and HFD-fed mice (n = 3/group). **(E,J,M)** The proportion of (E) CAF, (J) M1 and M2, and (M) T cell clusters in metastatic liver tumors of LFD-fed and HFD-fed mice. **(F,G)** Expression of *Has1*, *Has2*, *Has3*, and *Cd44* genes (columns) by specific CAF subpopulations (rows). Dot size represents the cell fraction within the CAF subpopulations. Fill color indicates average expression (ave. exp.). **(H,I)** CellChat receptor-ligand analysis of the predicted intercellular communication networks for cells from metastatic liver tumors of LFD-fed and HFD-fed mice. Arrows are proportional to the interaction strength between CAF2 and other cell clusters; node size is relative to the number of cells within that population. **(K,L)** Expression of *Cd44* and *Cd274* genes (columns) by specific M2 subpopulations (rows). Dot size represents the cell fraction within the M2 subpopulations. **(N,O)** Expression of key immunomodulatory genes (columns) by specific T cell subpopulations (rows). **(P)** The proposed model representing cancer YAP regulation of HSC-derived HAS2 for the immunosuppressive tumor microenvironment in steatotic liver. HA, hyaluronic acid; PD-1, programmed cell death protein 1; PD-L1, programmed death-ligand 1; TAM, tumor-associated macrophage.

Figure 6. Increased CAF infiltration and immunosuppressive TAM and T cell phenotypes in patients with CRC liver metastasis with steatotic liver.

(A) Representative images for hyaluronic acid binding protein (HABP) staining (left) and CTGF staining (right) using tissue microarray sections of metastatic colorectal cancer (CRC) patients. Scale bar: 200 μm. **(B)** Quantification of HABP-positive area. (Normal, *n* = 16; MASLD, *n* = 13) NT, nontumor; T, tumor. MASLD, metabolic dysfunction-associated steatotic liver disease. **(C)** Correlation between the HABP-positive area and the CTGF-positive area. Pearson correlation coefficient (r) was calculated. (Normal, NT, *n* = 15; MASLD, NT, *n* = 12; Normal, Tumor, *n* = 14; MASLD, Tumor, *n* = 11) **(D)** Representative imaging mass spectrometry (IMC) images for metastatic liver tumors for fibroblast activation protein (FAP), α-SMA, CD8, CD44, and CDX2 expression (left). Scale bars: 100 μm. Per-patient proportions of cancer-associated fibroblasts (CAFs) and α-SMA-positive CAFs (right). (Normal, *n* = 17; MASLD, *n* = 13) **(E,F)** Spatial analysis of IMC data to evaluate the density of CAFs surrounding (E) CD44-positive or -negative or (F) YAP-positive or -negative cancer cells. **(G,H)** Dot plot for expression of CD44, YAP, Ki67, and immunomodulatory molecules (columns) on (G) CD44-positive and -negative or (H) YAP-positive and -negative cancer cells (rows). Dot size represents the cell fraction within each cell population. Fill color indicates average expression (ave. exp.). PD-L1, programmed death-ligand 1. **(I)** Dot plot for expression of immunomodulatory molecules (columns) by macrophage subpopulations from patients with or without MASLD (rows). **(J,K)** Spatial analysis

of IMC data to evaluate the relationship between macrophage PD-L1 expression and (J) the macrophage's distance from CAFs or (K) the macrophage's density of CAFs. **(L)** Illustration of the proposed model. Data are shown as mean ± SEM (B,D) or mean ± SD (E,F,J,K). Statistical significance was calculated with one-way analysis of variance followed by Tukey post hoc test (B) or by two-tailed Student *t*-test (D) or generalized linear models (GLM) using the sample as a clustering variable to obtain robust standard error (E,F,J,K). *P* values are indicated ($^{*}P < 0.05$ or $^{**}P < 0.01$).

Figure 7. Inhibition of hyaluronic acid synthesis alleviates metastatic liver tumor growth and cancer-associated fibroblast activation in the steatotic liver disease condition.

(A) In vivo preventive experimental protocol. 4-methylumbelliferone (4-MU) was orally administered (PO) at 450 mg/kg, five times a week for four weeks, while 4-methylumbelliferyl glucuronide (4-MUG) was provided in drinking water at 2 mg/ml for four weeks. **(B)** Macroscopic appearance of the liver. Arrows indicate tumor sites. Veh, vehicle. **(C)** Analysis of maximal tumor diameter and number of nodules. (n = 6-9 per group) Scale bars: 1 cm. **(D)** Quantitative assessment of HABP, Sirius red, and α-SMA-positive areas. (n = 6-9 per group) **(E)** Measurement of mRNA expression levels for profibrogenic genes in HFD-fed mice treated with the respective drugs. (n= 6-8 per group) **(F)** Western blot analysis of mature collagen I and α-SMA. **(G)** Evaluation of mRNA expression levels for *Has1*, *Has2*, and *Has3*. (n = 6-8 per group) **(H)** In vivo treatment experimental protocol. **(I)** Macroscopic appearance of the liver from tumor-bearing mice. Scale bars: 1 cm. **(J)** Quantification of the maximal tumor diameter and the number of tumor nodules. (n = 7 per group) **(K)** Kaplan-Meier survival curves. Statistical significance was determined using the log-rank test (n = 8 per group). Data are presented as mean ± SEM. Statistical significance was calculated with one-way analysis of variance followed by Tukey post hoc test (C-E, G, J). *P* values are indicated (*$P < 0.05$ or **$P < 0.01$)

Figure 8. Improved effects of anti-PD-1 antibody treatment in combination with hyaluronic acid synthesis inhibition on metastatic liver tumor growth in the steatotic liver disease condition. (A) Experimental protocol for the in vivo combination treatment of 4-methylumbelliferone (4-MU) and anti-PD-1 antibody. 4-MU was administered orally (PO) at 450 mg/kg daily for 2 weeks, while anti-PD-1 antibody (200 μg) was administered intraperitoneally (IP) every 3 days for total 4 injections. (B) Analysis of maximal tumor diameter and number of nodules (n=8-9 per group). Data are presented as mean ± SEM. Statistical significance was calculated with one-way analysis of variance followed by Tukey post hoc test. *P* values are indicated ($^{**}P < 0.01$). (C) Macroscopic appearance of the liver. Arrows indicate tumor sites. Scale bar: 1 cm. IgG, control IgG.

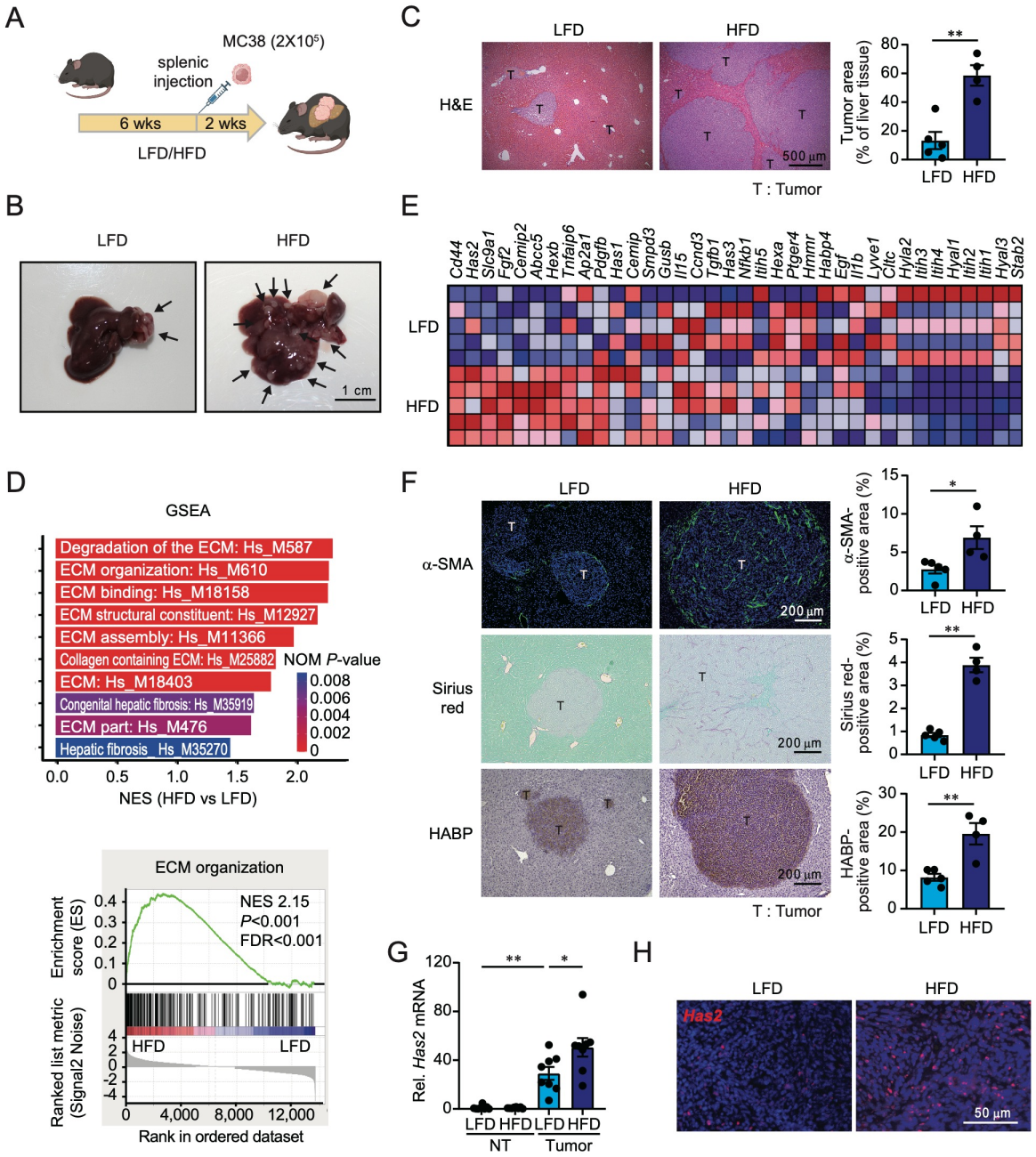

Figure 1. High-fat diet-induced steatotic liver increases HA accumulation and HAS2 expression in tumors.

(A) Representation of the mouse model illustrating the induction of steatotic liver and subsequent splenic injection of MC38 cells to form liver metastases. LFD, low-fat diet; HFD, high-fat diet. **(B)** Macroscopic appearance of the liver with arrows indicating tumor sites. Scale bar: 1 cm. **(C)** Representative images of hematoxylin and eosin (H&E)-stained tumor and quantitative assessment of tumor area based on H&E staining. (n = 4-5 per group) Scale bar: 500 µm. **(D)** RNA-seq analysis. Gene set enrichment analysis (GSEA) of gene expression for extracellular matrix (ECM) and liver fibrosis in tumors from mice fed an LFD or an HFD (upper). Enrichment plot for ECM organization (lower). FDR, false discovery rate; NES, normalized enrich ment score. NOM, nominal. **(E)** A heat map of the hyaluronic acid (HA)-related genes. (n = 5) **(F)** Representative microscopic images depicting liver sections stained for alpha-smooth muscle actin (α-SMA), with Sirius red, and for hyaluronic acid binding protein (HABP). Scale bars: 200 µm. Quantification of α-SMA-positive area, Sirius red-positive area, and HABP-positive area. (n = 4-5 per group) **(G)** Comparison of mRNA expression levels of *Has2* in nontumor (NT) and tumor tissues from mice fed an LFD or an HFD. (n = 8 per group) **(H)** Representative images of RNAscope *in situ* hybridization for *Has2*. Data are presented as mean ±SEM. Statistical significance was calculated with Student t-test (C, F) and one-way analysis of variance followed by Tukey post hoc test (G). P values are indicated (*P< 0.05 or **P< 0.01).

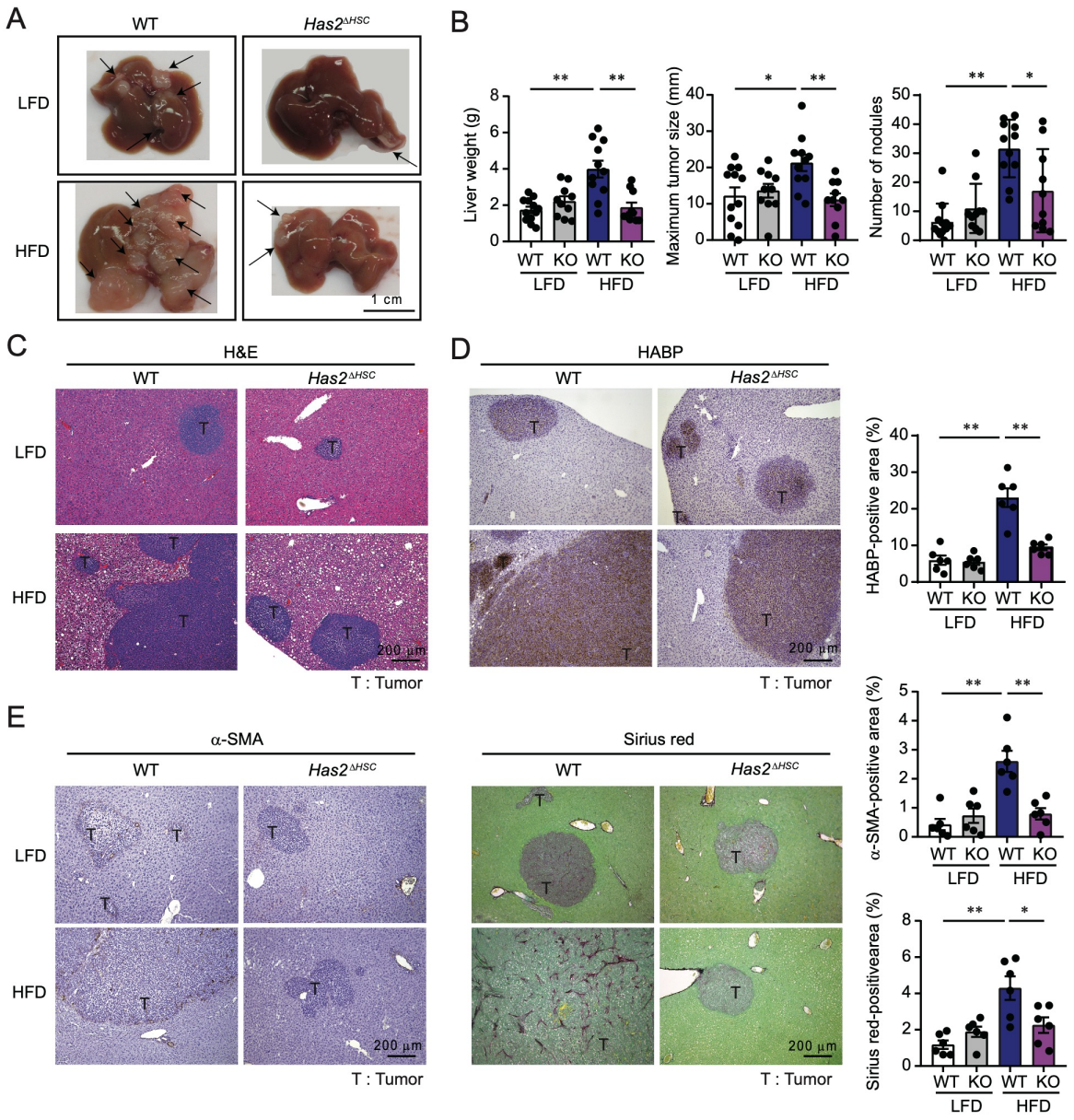

Figure 2. Suppression of metastatic liver tumor growth enhanced by metabolic dysfunction-associated steatotic liver disease through HSC-specific Has2 deficiency.

(A) Macroscopic appearance of the liver. Wild-type (WT) and *Has2*$^{\Delta HSC}$ mice were intrasplenically injected with MC38 cells after 6 weeks of either low-fat diet (LFD) or high-fat diet (HFD) feeding. Mice were maintained on their respective diets for an additional 2 weeks. Arrows indicate the tumors. Scale bar: 1 cm. **(B)** Measurement of liver weight, maximal tumor diameter, and number of nodules. (n = 10-12 per group) KO, knockout. **(C)** Representative images of hematoxylin and eosin (H&E) staining of liver tissue sections. Scale bar: 200 μm. **(D)** Representative images and quantification of hyaluronic acid binding protein (HABP) staining (n = 6). Scale bar: 200 μm. **(E)** Representative images and quantification of immunostaining with alpha-smooth muscle actin (α-SMA) and Sirius red staining of liver tissue sections (n = 6). Scale bar: 200 μm. Data are presented as mean ± SEM. Statistical significance was calculated with one-way analysis of variance followed by Tukey post hoc test. P values are indicated (*P < 0.05 or **P < 0.01).

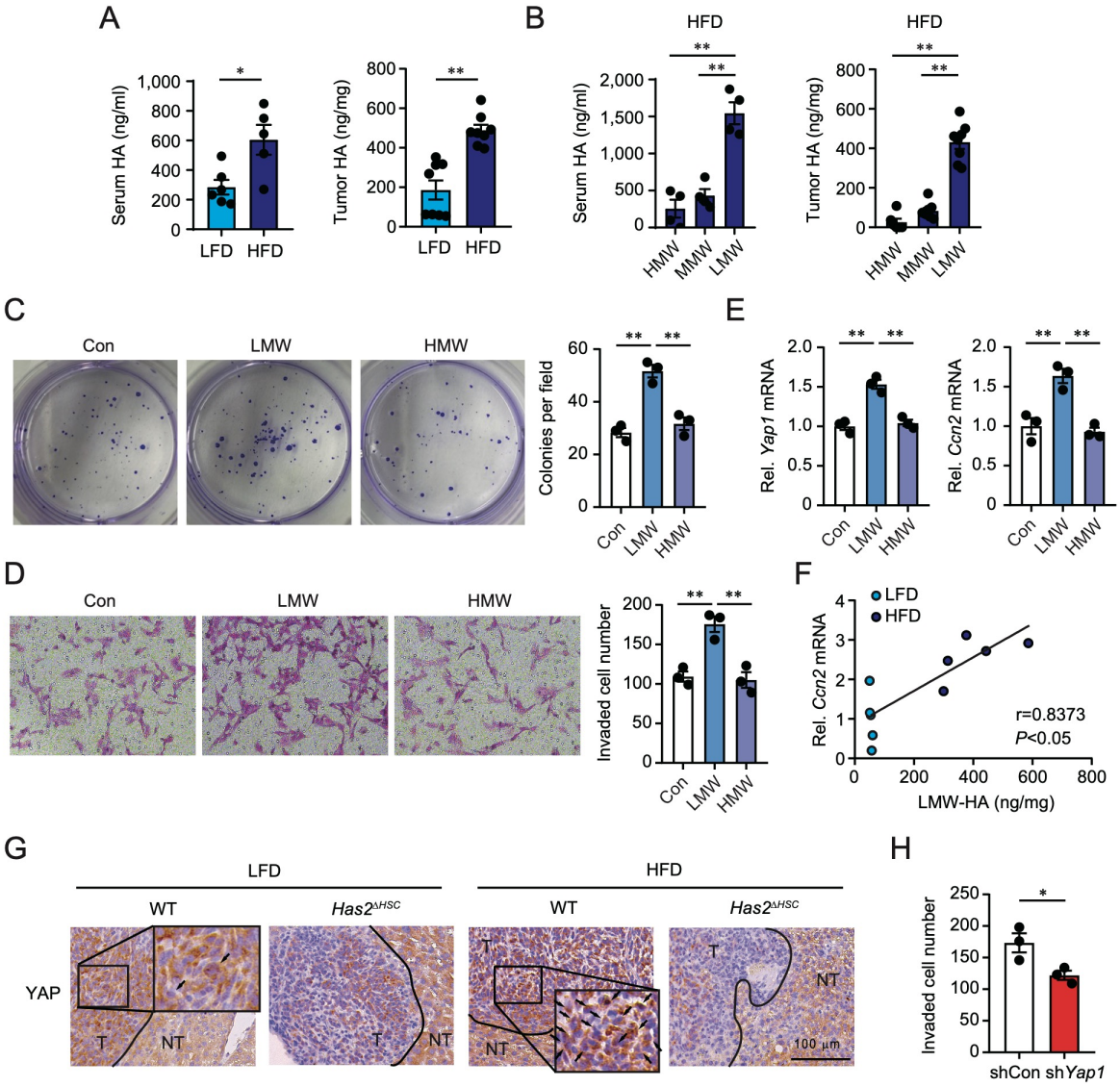

Figure 3. HAS2 and low molecular weight HA play an important role in cancer cell aggressiveness and YAP activation.

(A) Serum hyaluronic acid (HA) levels (left) and tumor HA levels (right) between tumor-bearing mice on a low-fat diet (LFD) and those on a high-fat diet (HFD). (serum, n = 5-6 per group; tumor, n = 8 per group) **(B)** Fractionated analysis of HA content, distinguishing between high-molecular weight (HMW)-HA (>300 kDa), medium molecular weight (MMW)-HA (100~300 kDa), and low-molecular weight (LMW)-HA (<100 kDa). Serum and tissue homogenate samples from HFD-fed, tumor-bearing mice were fractionated using columns. (serum, n = 4; tumor, n = 8) **(C)** The influence of LMW-HA and HMW-HA on the colony formation and **(D)** invasion ability of MC38 cells. (n = 3) **(E)** The effect of LMW-HA and HMW-HA on *Yap1* and *Ccn2* mRNA expression in MC38 cells. (n = 3) Con, control. **(F)** The correlation between LMW-HA levels and *Ccn2* mRNA expression in tumors from mice on an LFD and an HFD. The Pearson correlation coefficient (r) was calculated. (n = 5) **(G)** Effect of hepatic stellate cell (HSC)-specific *Has2* deletion on YAP expression in tumors from wild-type (WT) mice or knockout (KO) mice. (n = 8) Representative images of YAP staining were shown. NT, nontumor; T, tumor. **(H)** The effect of *Yap1* knockdown in MC38 cells on LMW-HA-induced cancer cell invasion. The number of invaded cells per field are is shown. (n = 3) Sh, short hairpin. Data are presented as mean ± SEM. Statistical significance was calculated with Student t-test (A, H) and one-way analysis of variance followed by Tukey post hoc test (B-E). P values are indicated (*P < 0.05 or **P < 0.01).

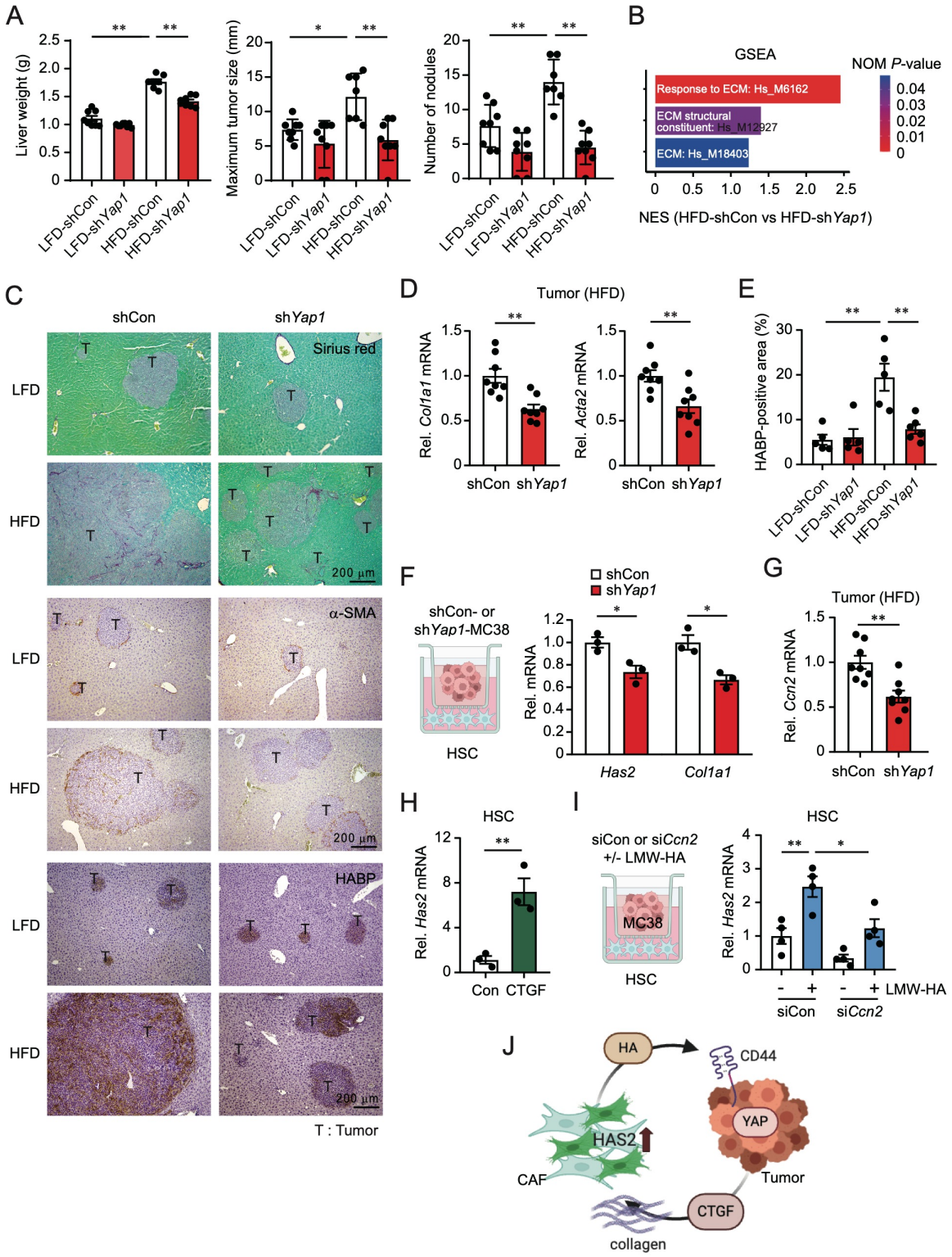

Figure 4. YAP knockdown attenuates colorectal cancer aggressiveness and cancer-associated fibroblast activation.

(A) Following six weeks of low-fat diet (LFD) or high-fat diet (HFD) feeding, MC38 cells with either shCon or sh*Yap1* were intrasplenically injected into mice. Liver weight (left), maximum tumor size (middle), and number of nodules (right) (n = 7-8 per group). **(B)** Gene set enrichment analysis. NES, normalized enrichment score. NOM, nominal. **(C)** Representative Sirius red (upper), α-SMA (middle), and hyaluronic acid binding protein (HABP) (lower) in metastatic liver tumors. **(D)** mRNA expression of *Col1a1* and *Acta2* in tumor tissues. (n = 8) **(E)** Quantification of HABP-positive area. (n = 5-6 per group) **(F)** Co-culture experiments. *Has2* and *Col1a1* mRNA levels in mouse primary hepatic stellate cells (HSCs) ShCon-MC38 or sh*Yap1*-MC38 cells were placed in the upper chamber and primary HSCs were seeded in the lower chamber. (n = 3) **(G)** *Ccn2* mRNA levels in tumor tissues. (n = 8) **(H)** CTGF treatment in primary HSCs. (n = 3) **(I)** *Has2* mRNA levels in mouse primary HSCs. MC38 cells were transiently transfected with siCon or si*Ccn2* and treated with vehicle or LMW-HA. MC38 cells were loaded in the upper chamber. HSCs were seeded in the lower chamber one day before coculture. Coculture lasted 48 hours. (n = 4) **(J)** Illustration showing the bidirectional regulation between HSC and CRC. Data are presented as mean ± SEM. Statistical significance was calculated with Student t-test (D, F, G, H) and one-way analysis of variance followed by Tukey post hoc test (A, E, I). P values are indicated (*P< 0.05 or **P< 0.01).

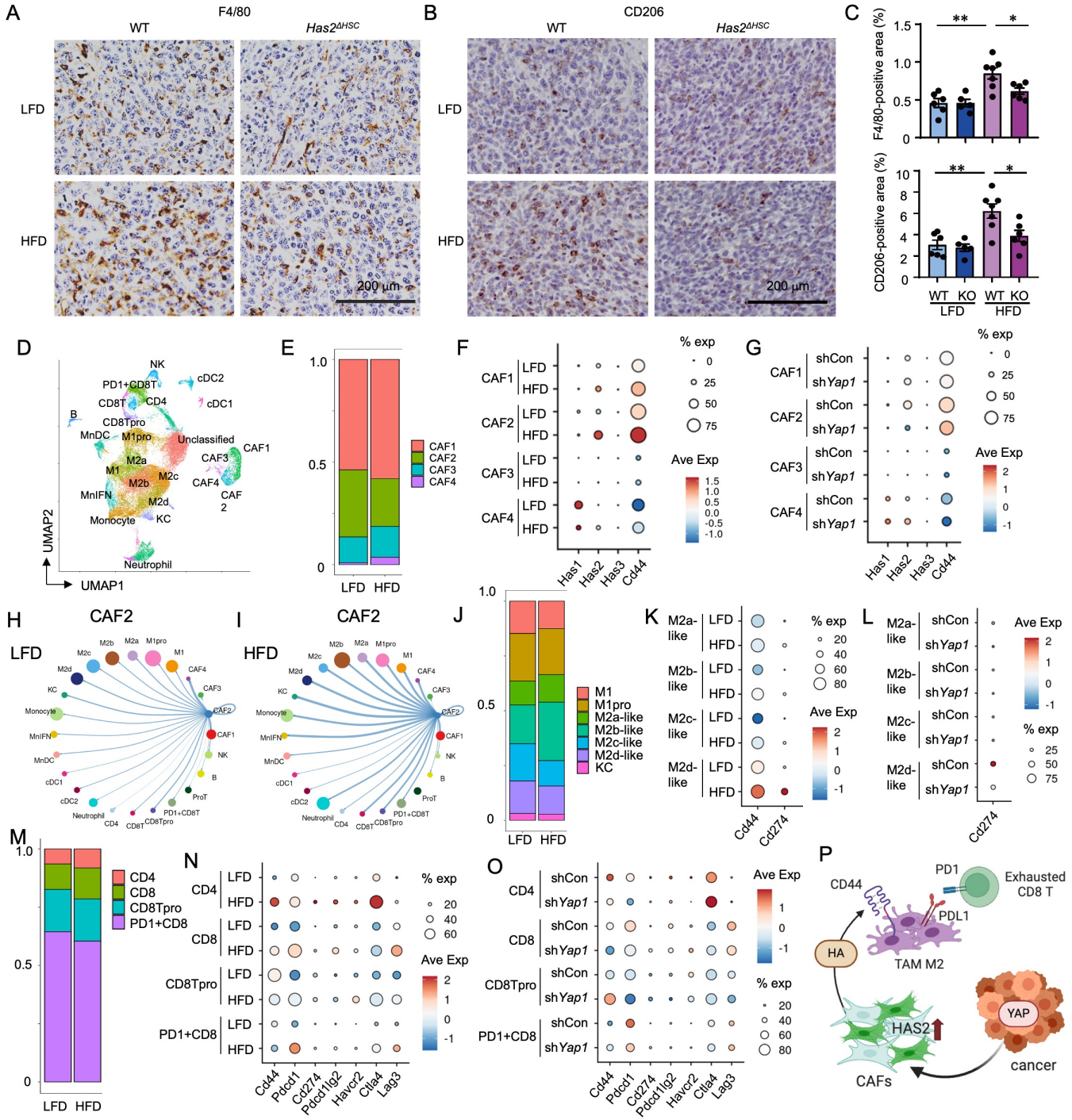

Figure 5. CAF-derived HAS2 and cancer-derived YAP contribute to a prometastatic immune tumor microenvironment in steatotic liver.

(A,B) Representative immunohistochemistry images for (A) F4/80 and (B) CD206 from tumors in Figure 2. HFD, high-fat diet; HSC, hepatic stellate cell; LFD, low-fat diet. Scale bar: 200μm. **(C)** Quantification of F4/80+ (upper) and CD206+ (lower) areas. (n = 5-7 per group). Data are presented as mean ± SEM. Statistics, one-way ANOVA with Tukey post hoc test. **(D)** Tumor-infiltrating cancer-associated fibroblast (CAF) and immune cell populations. UMAP of single-cell RNA-seq from 46,577 cells showing 25 clusters determined by integrated analysis, colored by cluster. Cells were from metastatic liver tumors of LFD-fed and HFD-fed mice (n = 3/group). **(E,J,M)** The proportion of (E) CAF, (J) M1 and M2, and (M) T cell clusters in metastatic liver tumors of LFD-fed and HFD-fed mice. **(F,G)** Expression of *Has1*, *Has2*, *Has3*, and *Cd44* genes (columns) by specific CAF subpopulations (rows). Dot size, the cell fraction within the CAF subpopulations. Fill color, average expression (ave. exp.). **(H,I)** CellChat receptor-ligand analysis of the predicted intercellular communication networks for cells from metastatic liver tumors of LFD-fed and HFD-fed mice. Arrows are proportional to the interaction strength between CAF2 and other cell clusters; node size is relative to the number of cells within that population. **(K,L)** Expression of *Cd44* and *Cd274* genes (columns) by specific M2 subpopulations (rows). Dot size, the cell fraction within the M2 subpopulations. **(N,O)** Expression of key immunomodulatory genes (columns) by specific T cell subpopulations (rows). **(P)** The proposed model representing cancer YAP regulation of HSC-derived HAS2 for the immunosuppressive tumor microenvironment in steatotic liver. HA, hyaluronic acid; TAM, tumor-associated macrophage.

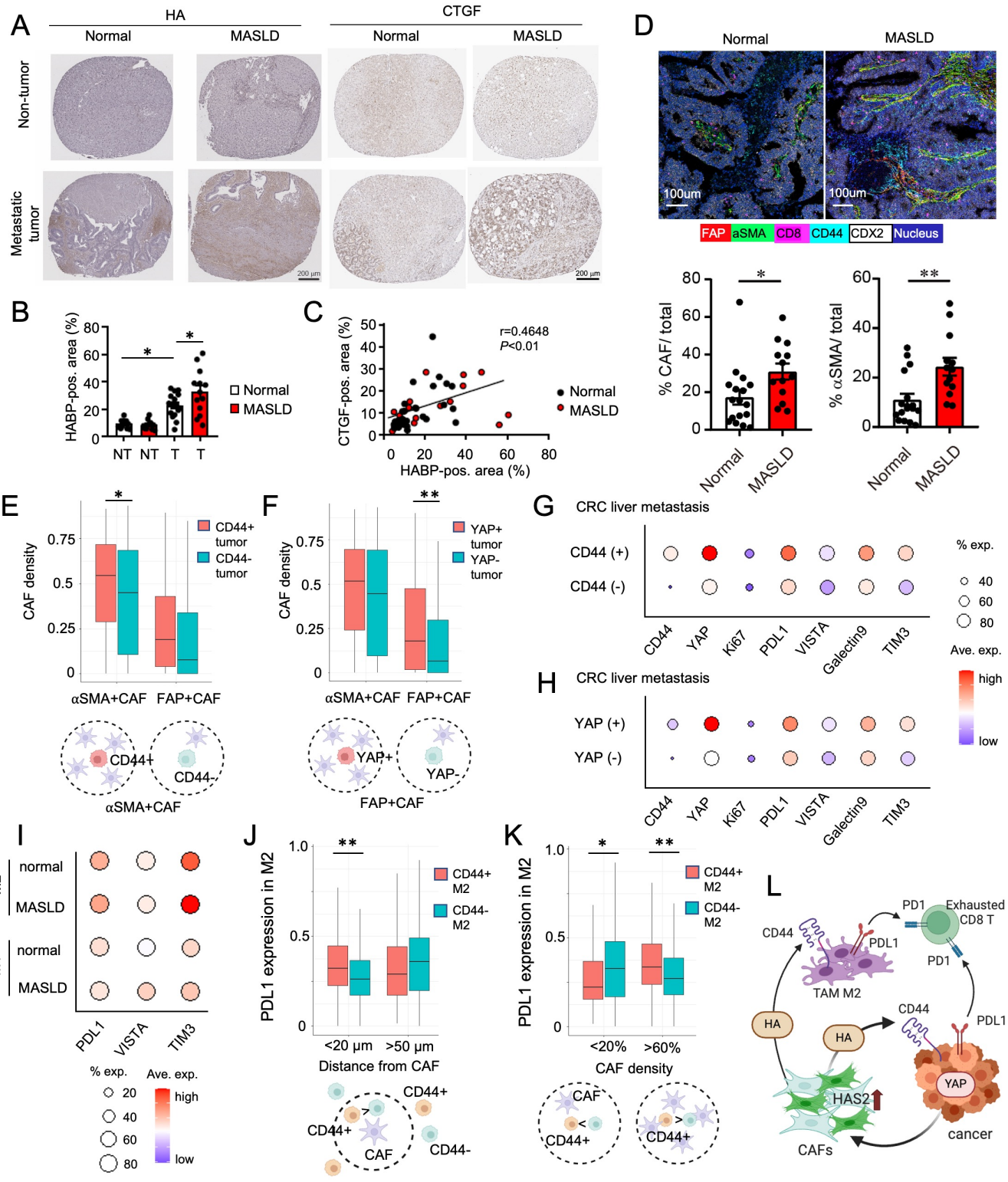

Figure 6. Increased CAF infiltration and immunosuppressive TAM and T cell phenotypes in patients with CRC liver metastasis with steatotic liver. (A) Representative images for hyaluronic acid (HA) and CTGF staining using tissue microarray of metastatic colorectal cancer (CRC) patients. Scale bar: 200μm. **(B)** Quantification of HA area. (Normal, $n = 16$; MASLD, $n = 13$) NT, nontumor; T, tumor. . **(C)** Correlation between HA area and CTGF area. Pearson correlation coefficient (r) was calculated. **(D)** Representative imaging mass spectrometry (IMC) images for metastatic liver tumors. Scale bars: 100μm. Per-patient proportions of cancer-associated fibroblasts (CAFs) and αSMA+ CAFs. (Normal, n=17; MASLD, n=13) **(E,F)** Spatial analysis of IMC data for the density of CAFs surrounding (E) CD44+/- or (F) YAP+/- cancer cells. **(G,H)** Dot plot for CD44, YAP, Ki67, and immunomodulatory molecules (columns) on (G) CD44+/- or (H) YAP+/- cancer cells (rows). Dot size, the cell fraction within each cell population. Fill color, average expression. **(I)** Dot plot for immunomodulatory molecules (columns) by macrophage subpopulations from patients with or without MASLD (rows). **(J,K)** Spatial analysis of IMC data to evaluate the relationship between macrophage PD-L1 and (J) the macrophage's distance from CAFs or (K) the macrophage's density of CAFs. **(L)** Illustration of the proposed model. Data are shown as mean ± SEM (B,D) or mean ± SD (E,F,J,K). Statistical significance was calculated with one-way analysis of variance followed by Tukey post hoc test (B) or by two-tailed Student t-test (D) or generalized linear models (GLM) using the sample as a clustering variable to obtain robust standard error (E,F,J,K). P values are indicated ($^{*}P < 0.05$ or $^{**}P < 0.01$).

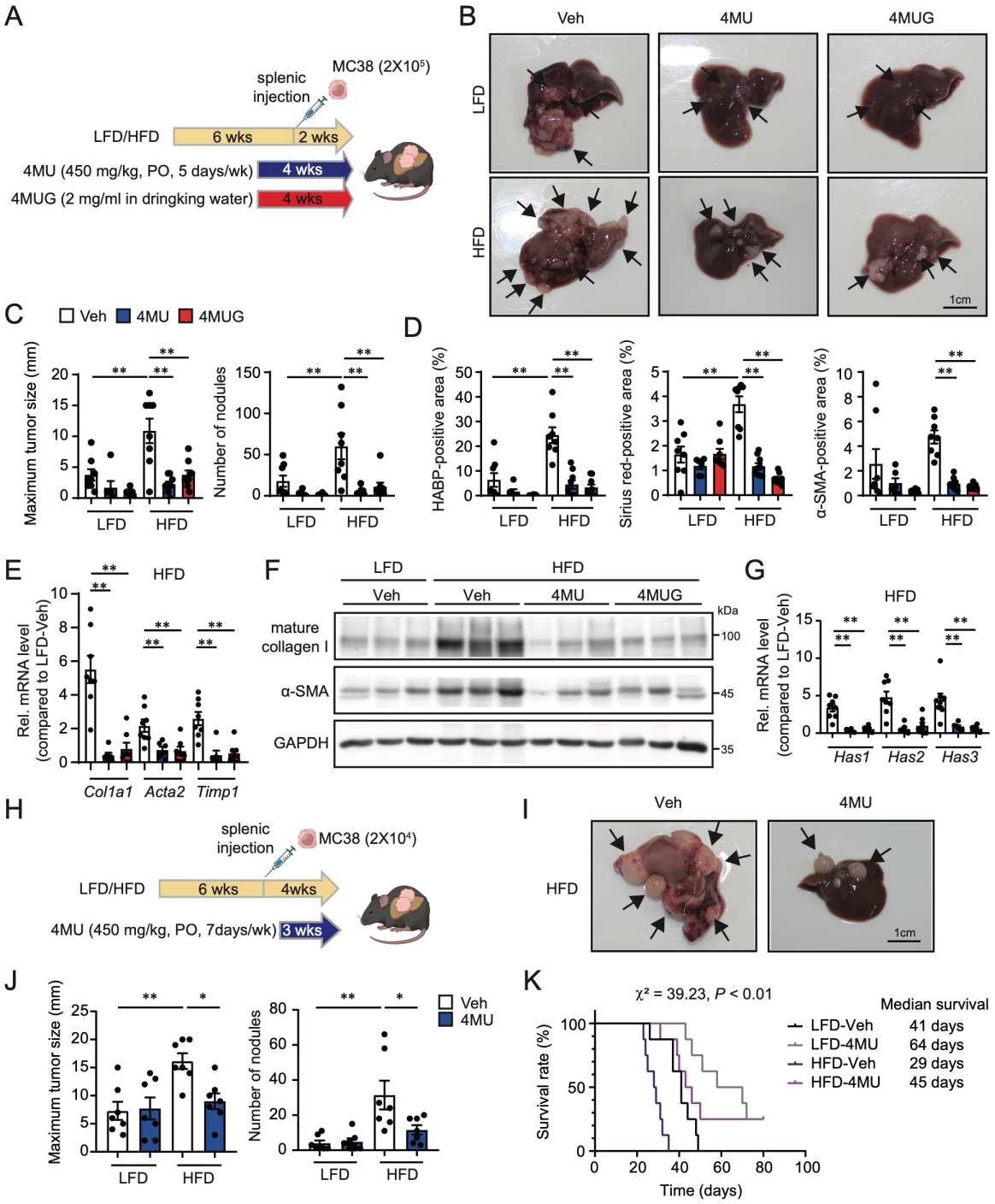

Figure 7. Inhibition of hyaluronic acid synthesis alleviates metastatic liver tumor growth and cancer-associated fibroblast activation in the steatotic liver disease condition.

(A) In vivo preventive experimental protocol. 4-methylumbelliferone (4-MU) was orally administered (PO) at 450 mg/kg, five times a week for four weeks, while 4-methylumbelliferyl glucuronide (4-MUG) was provided in drinking water at 2 mg/ml for four weeks. **(B)** Macroscopic appearance of the liver. Arrows indicate tumor sites. Veh, vehicle. **(C)** Analysis of maximal tumor diameter and number of nodules. (n = 6-9 per group) Scale bars: 1 cm. **(D)** Quantitative assessment of HABP, Sirius red, and α-SMA-positive areas. (n = 6-9 per group) **(E)** Measurement of mRNA expression levels for profibrogenic genes in HFD-fed mice treated with the respective drugs. (n= 6-8 per group) **(F)** Western blot analysis of mature collagen I and α-SMA. **(G)** Evaluation of mRNA expression levels for *Has1*, *Has2*, and *Has3*. (n = 6-8 per group) **(H)** In vivo treatment experimental protocol. **(I)** Macroscopic appearance of the liver from tumor-bearing mice. Scale bars: 1 cm. **(J)** Quantification of the maximal tumor diameter and the number of tumor nodules. (n = 7 per group) **(K)** Kaplan-Meier survival curves. Statistical significance was determined using the log-rank test (n = 8 per group). Data are presented as mean ± SEM. Statistical significance was calculated with one-way analysis of variance followed by Tukey post hoc test (C-E, G, J). P values are indicated (*P < 0.05 or **P < 0.01)

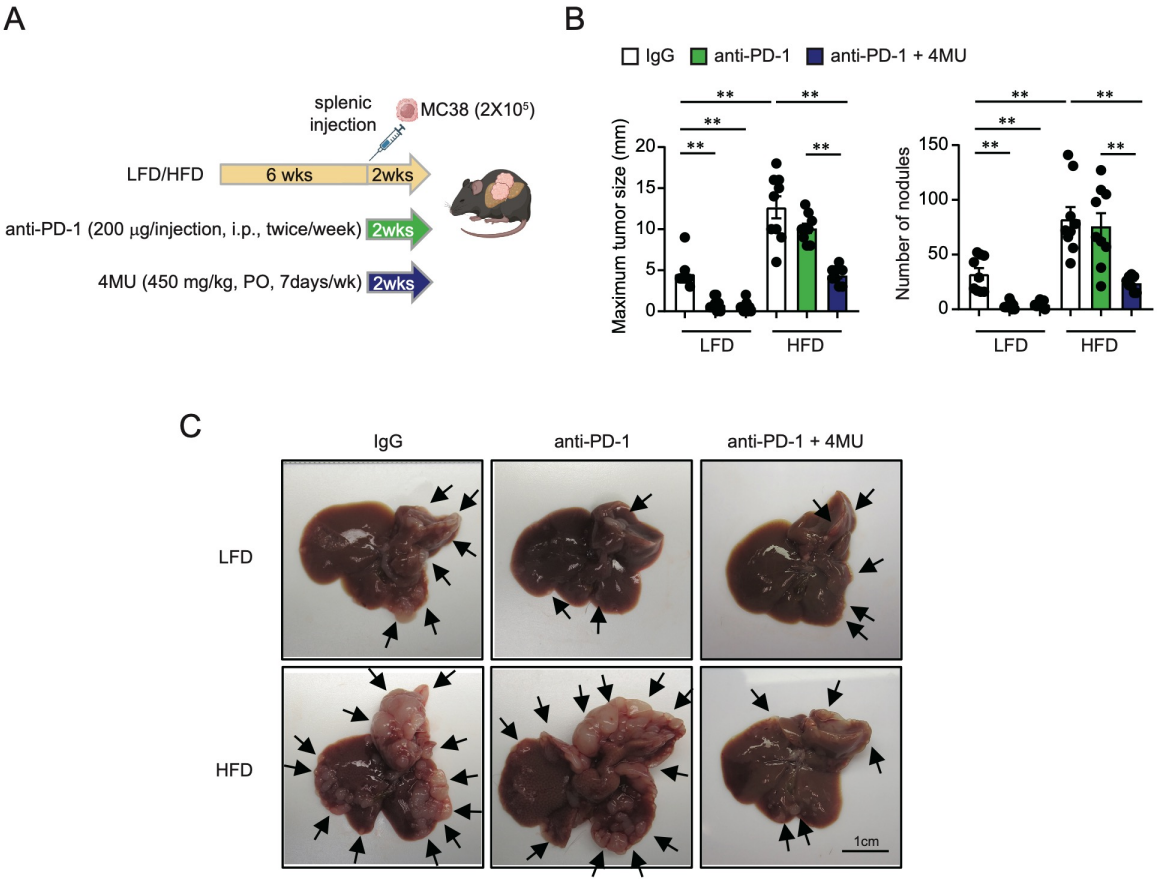

Figure 8. Improved effects of anti-PD-1 antibody treatment in combination with hyaluronic acid synthesis inhibition on metastatic liver tumor growth in the steatotic liver disease condition.

(A) Experimental protocol for the in vivo combination treatment of 4-methylumbelliferone (4-MU) and anti-PD-1 antibody. 4-MU was administered orally (PO) at 450 mg/kg daily for 2 weeks, while anti-PD-1 antibody (200 μg) was administered intraperitoneally (IP) every 3 days for total 4 injections. **(B)** Analysis of maximal tumor diameter and number of nodules (n = 8-9 per group). Data are presented as mean ± SEM. Statistical significance was calculated with one-way analysis of variance followed by Tukey post hoc test. P values are indicated (**$P < 0.01$). **(C)** Macroscopic appearance of the liver. Arrows indicate tumor sites. Scale bar: 1 cm. IgG, control IgG.